Improving the Xin'anjiang Hydrological Model Based on Mass-Energy Balance

Yuan-Hao Fang[1,2,4], Xingnan Zhang[1,2,3], Chiara Corbari[4], Marco Mancini[4], Guo-Yue Niu[5,6], and Wenzhi Zeng[7,8]

[1]National Cooperative Innovation Center for Water Safety & Hydro-Science, Hohai University, Nanjing, China
[2]College of Hydrology and Water Resources, Hohai University, Nanjing, China
[3]National Engineering Research Center of Water Resources Efficient Utilization and Engineering Safety, Hohai University, Nanjing, China
[4]Department of Civil and Environmental Engineering (D.I.C.A.), Politecnico di Milano, Milan, Italy
[5]Department of Hydrology and Atmospheric Sciences, University of Arizona, Tucson AZ, U.S.A
[6]Biosphere 2, University of Arizona, Oracle AZ, USA
[7]State Key Laboratory of Water Resources and Hydropower Engineering Science, Wuhan University, Wuhan, China
[8]Crop Science Group, Institute of Crop Science and Resource Conservation (INRES), University of Bonn, Bonn, Germany

Correspondence to: Xingnan Zhang (zxn@hhu.edu.cn)
Chiara Corbari (chiara.corbari@polimi.it)

Abstract. Conceptual hydrological models are preferable for real-time flood forecasting, among which the Xin'anjiang (XAJ) model has been widely applied in humid and semi-humid regions of China. Although the relatively simple mass balance scheme ensures a good performance of runoff simulation during flood events, the model still has some defects. Previous studies have confirmed the importance of Evapotranspiration (ET) and soil moisture content (SMC) in runoff simulation. In

5   order to add more constraints to the original XAJ model, an energy balance scheme suitable for the XAJ model was developed and coupled with the original mass balance scheme of the XAJ model. The detailed parameterizations of the improved model, XAJ-EB, are presented in the first part of this paper. XAJ-EB employs various meteorological forcing and remote sensing data as input, simulating ET and runoff yield using a more physically-based mass-energy balance scheme. In particular, the energy balance is solved by determining the representative equilibrium temperature (RET), which is comparable to land surface

10   temperature (LST). The XAJ-EB was evaluated in the Lushui catchment situated in the middle reach of the Yangtze River Basin for the period between 2004 and 2007. Validation using ground-measured runoff data proves that the XAJ-EB is capable of reproducing runoff comparable to the original XAJ model. Additionally, RET simulated by XAJ-EB agreed well with Moderate Resolution Imaging Spectroradiometer (MODIS) retrieved LST, which further confirms that the model is able to simulate the mass-energy balance since LST reflects the interactions among various processes. The validation results prove that the XAJ-EB

15   model has superior performance compared with the XAJ model and also extends its applicability.

1 Introduction

Hydrological models are widely used for real-time flood forecasting due to their abilities to predict hydrological fluxes (e.g. runoff) and states (e.g. soil moisture) with various leading time (Chen et al., 2016). These models can be grouped as physically-

based models which are mainly based on partial differential equations (e.g. Richards equation, de St. Venant equation, etc.) or conceptual models which usually employ a number of mathematical functions or distribution curves to reproduce hydrological processes (Kampf and Burges, 2007; Niu et al., 2014). Conceptual models are preferred for flood forecasting with consideration of the data and computational conditions (Blöschl et al., 2008; Hapuarachchi et al., 2011). Examples are the Sacramento soil

5   moisture accounting (SAC-SMA) model (Burnash et al., 1973) implemented by the US National Weather Service (NWS) (Smith et al., 2003); a spatially distributed flash flood model used in northern Austria (Blöschl et al., 2008); the HBV model (Bergström et al., 1995; Zhang and Lindström, 1997) adopted for the forecasting of Savinja catchment (Kobold and Brilly, 2006), and the Xin'anjiang (XAJ) model (Zhao, 1995) applied in the Huaihe river basin, China (Lu et al., 2008). These operational practices have proved the accuracy of stream discharge predicted by conceptual models, which is usually the major

10   concern of real-time flood forecasting.

In China, the XAJ model is the most widely used model for flood forecasting in humid and semi-humid regions (Liu et al., 2009; Yao et al., 2009; Zhao, 1992). The XAJ model employs a spatial probability distribution curve to represent the variability of tension water capacity in the catchment and calculates runoff generation based on the conception of mass balance (Zhao, 1995). With respect to the evapotranspiration (ET), the XAJ model uses pan evaporation as its input, and then computes actual

15   ET using an empirical relationship, taking only the soil moisture content (SMC) into account. Such a generalized scheme successfully strikes a balance between model complexity and computational accuracy, providing a reasonable runoff prediction during flood events after proper calibration against runoff observations.

At present, however, the traditional calibration approach is becoming more challenging for the XAJ model. This is partly due to the fact that the model parameters have become distributed to take account of the heterogeneities of the catchment (Xia and

20   Zhang, 2009; Yao et al., 2012), which theoretically requires more constraints to calibrate and validate these spatially-distributed parameters.

Moreover, although precipitation and runoff can be measured by traditional approaches, accurate catchment average ET and SMC are difficult to obtain at the catchment scale. Therefore the bias of simulations is more likely to be accumulated in SMC when only mass balance is considered. The significance of SMC to real-time flood forecasting has gradually been recognized.

25   Studies showed that the bias in predicting flood peaks is related to unrealistic antecedent SMC estimation (Huza et al., 2014), and therefore the performance of real-time flood forecasting can be improved by setting or assimilating initial SMC (Brocca et al., 2009; Berthet et al., 2009; Komma et al., 2008; Tramblay et al., 2010; Wanders et al., 2014). The accuracy of SMC estimation before flood events largely depends on ET estimation. In addition, considering the abilities to extend the leading time and quantify predictability, ensemble flood forecasting techniques are more attractive today (Cloke and Pappenberger,

30   2009), and the estimation of SMC and ET is even more important in ensemble flood forecasting due to a longer leading time.

For the aforementioned reasons, it is therefore necessary to introduce more constraints to the XAJ model, and the energy balance can serve this purpose well since the hydrological processes are governed by both mass and energy balance. One feasible way to introduce the energy balance to the XAJ model is through ET. As is discussed before, the simple and empirical ET routine of the XAJ model is based on mass balance only, and the major defects of the ET routine are: (1) the input pan

35   evaporation is measured only at few specific locations, reflecting daily evaporation from open water, which means that the

potential ET (PET) over a large area is assumed to be the same. Such an assumption dose not always hold under heterogeneous meteorology or underlying surface conditions (Xu et al., 2006; Yuan et al., 2008); (2) calibration of K_c (see Section 2.1 for details), a sensitive parameter of the XAJ model controlling water balance, is needed to convert pan evaporation to PET, which is impossible for ungauged catchments where observed runoff is unavailable; and (3) the empirical relationship linking PET with actual ET only takes water balance into account, neglecting other factors (e.g. meteorological conditions) that control ET processes (Wang and Dickinson, 2012).

It needs noted that the energy balance-based ET schemes have been intensively studied in the land surface modeling community (Overgaard et al., 2006). Land surface models (LSMs) are developed to provide various fluxes and states connecting the atmosphere and land surface (Overgaard et al., 2006; Niu et al., 2011). Most LSMs have an energy balance component for ET estimation, but the way these models solve the energy balance differs. According to Su (2002) and Kalma et al. (2008), generally three different approaches are employed by LSMs for ET estimation: (1) calculate all energy balance components except latent heat flux, which is obtained as the residual of the energy budget; (2) compute all components involved in energy balance by closing the balance equation, latent heat is solved at the same time when energy budget is closed; and (3) an empirical approach using water stress to derive ET. However, these approaches are rarely applied in hydrological models,especially for real-time flood forecasting, because their structures are complex and generally require considerable data and parameters to drive the model.

Benefiting from remote sensing and data assimilation techniques, more meteorological and land surface data are available now. The scientific community has been working to improve ET scheme of hydrological models (e.g. Corbari et al., 2011; Niu et al., 2014; Spies et al., 2015; Yan et al., 2012). In particular, some efforts have been made to improve the ET simulation of the XAJ model. Methodologies reported can be summarized as two approaches. The first approach was to introduce a physically-based formula to simulate PET based on meteorological measurements, aiming to provide more accurate PET input while the XAJ model structure remained unchanged (Yuan et al., 2008). The second approach involved replacing the ET routine by a more sophisticated scheme, typically the Penman-Monteith (PM) equation, which simulates actual ET by meteorological variables, remote sensing data and modeled SMC (Li et al., 2009; Zhou et al., 2013). These studies have demonstrated the feasibility of improving the ET scheme of the XAJ model. In these previous work, however, the mass balance and energy balance are either isolated or one-way linked, neglecting the interactions between them. Additionally, the PM equation employed tends to neglect evaporation due to the "big leaf" assumption (Yan et al., 2012). A more scientific way to simulate ET is by coupling both the mass and energy. For example, as reported by Corbari et al. (2011), a water balance model FEST (Rabuffetti et al., 2008) was augmented by coupling a energy balance scheme and various case studies have confirmed its applicability under different conditions (Masseroni et al., 2011; Corbari et al., 2013; Corbari and Mancini, 2014).

The overall goal of this paper is to develop an energy balance scheme suitable for the XAJ model, with which the mass balance-based runoff yield scheme of the original XAJ model can be fully coupled. The improved model employs a physically-based mass-energy balance component to simulate ET and runoff yield, imposing more constrains on the XAJ model. The remainder of the paper is organized as follows: Section 2 presents the basic theory we adopted to develop the mass-energy

balance scheme for the XAJ model; Section 3 reports the calibration and validation of the improved model against various observations; Section 4 further discusses the advantages of the improved model and Section 5 summarizes the study.

2   Improving the XAJ model

2.1   the XAJ Model and Its Mass Balance Scheme

5   The XAJ model was developed by Zhao (1977, 1995) based on the concept of runoff formation with respect to repletion of storage, which means that for each location in the catchment, there is no runoff yielded until the soil water deficit is replenished. Therefore, the XAJ model is the most suitable for humid and semi-humid regions where saturation-excess runoff is more likely to occur. A statistical tension water capacity curve was introduced to represent the spatial distribution of tension water capacity (maximum soil water deficit, i.e. the difference between field capacity and wilting point), which is regarded as the essence of 10   the XAJ model. The flow chart of the XAJ model is shown in Figure 1. All symbols outside the blocks are parameters, whose physical meanings are shown in Table 1. The inputs to the model are areal mean rainfall (P) and measured pan evaporation (EM) while the outputs are the discharge at the outlet of the basin (TQ) and the actual ET.

Figure 1 here

Table 1 here

15   The basic computational unit of the XAJ model is the element area, which, in principal, is a small natural catchment that has relatively homogeneous underlying surface characteristics (e.g. terrain, soil and vegetation, etc.). Simulation of outflow from each element area consists of 4 major components (Li et al., 2011; Qu et al., 2011). Here we only present a simple description; for mote details, refer to Zhao (1992):

(1) Evapotranspiration, which is simulated by a three-layer soil (i.e. upper, lower, and deep layer) model based on pan 20   evaporation and soil moisture;

(2) Runoff yield, which, based on the tension water capacity curve, simulates the runoff yield according to the rainfall and soil storage deficit;

(3) Runoff separation, which separates the abovementioned runoff into three components, i.e., surface, subsurface, and groundwater;

25   (4) Flow routing, which transfers the local runoff to the outlet of each basin forming the outflow. Several approaches including a unit hydrograph, linear reservoir, and lag & route can be adopted.

The mass balance of the XAJ model is expressed as:

$$\Delta W = P - R - ET \tag{1}$$

where ΔW is the soil water content storage term (mm); P is precipitation (mm); and R is runoff yield (mm).

The mass balance solution depends on the non-linear relationship between W and R represented by a tension water capacity curve (Figure 2), for a given time step when P is larger than ET, R is calculated as:

$$R = P - ET - (WM - W_0) + WM\left(1 - \frac{P - ET + A}{WMM}\right)^{1+B} \qquad (P - ET + A < WMM) \qquad (2)$$

$$R = P - ET - (WM - W_0) \qquad (P - ET + A \geqslant WMM) \qquad (3)$$

where W_0 is the initial soil water (mm), A is the value of Y axis of the tension water capacity curve corresponding to W_0 (mm), WMM is the maximum tension water capacity over the catchment (mm); and WM and B are parameters of the XAJ model as listed in Table 1.

Figure 2 here

2.2 Energy Balance Scheme Developed for the XAJ model

The energy balance of land surface is expressed as:

$$\Delta S = R_n - G - H - LE \qquad (4)$$

where ΔS is the energy storage term (W m^{-2}); R_n is net radiation (W m^{-2}); G is ground heat flux (W m^{-2}); H is sensible heat flux (W m^{-2}); and LE is latent heat flux (W m^{-2}).

In this paper, a "patch approach" was adopted to distinguish the energy fluxes between bare soil and the canopy (Lhomme and Chehbouni, 1999; Lu et al., 2014), assuming both bare soil and the canopy receive the same radiation loading, and the total sensible and latent heat fluxes are weighted by the canopy fraction f_v derived from leaf area index (LAI):

$$f_v = 1 - e^{-0.52LAI} \qquad (5)$$

1. **Net radiation (R_n)**

   R_n is the arithmetic difference between downward and upward short and long wave radiation:

$$R_n = R_{ds}(1 - \alpha) + R_{dl} - \zeta\sigma(RET^4) \qquad (6)$$

   where R_{ds} and R_{dl} are downward short and long wave radiation (W m^{-2}), respectively; α is land surface Albedo (-); ζ is land surface emissivity (-); σ is the Stefan-Boltzmann constant (W m^{-2} K^{-4}); and RET is representative equilibrium temperature (K).

2. **Ground heat flux (G)**

   G is the flux that is transferred between the land surface and the subsurface via soil thermal conduction:

$$G = (k_s/dz)(RET - T_{soil}) \qquad (7)$$

Where k_s is soil thermal conductivity (W m^{-1} K^{-1}), which is related to soil conditions (Corbari et al., 2011; McCumber and Pielke, 1981); dz is the soil depth for calculating ground heat flux (m); and T_{soil} is soil temperature at depth dz (K).

Eq.(7) can be solved numerically together with the heat diffusion equation as implemented by many LSMs; however, such an approach requires detailed thermal and hydrological information on different soil layers which is not available in the XAJ model. In addition to the numerical solution, there are also other parameterizations that derive G from more easily available data, e.g. net radiation (Idso et al., 1975; Santanello and Friedl, 2003; Su, 2002), sensible heat flux (Cellier et al., 1996) or surface temperature (Bhumralkar, 1975; Deardorff, 1978; Wang and Bras, 1999). Liebethal and Foken (2007) and Venegas et al. (2013) evaluated different approaches and found these alternatives can also reproduce reasonable G after calibration. In order to accommodate the energy balance scheme, we adopted force restore model proposed by Bhumralkar (1975) and Blackadar (1976) to estimate G from RET, the original force restore equation to estimate soil temperature can be rearranged as:

$$G = \frac{1}{C_T}\left[\frac{(RET - RET_0)}{\Delta t} + \frac{2\pi}{\tau}(RET - \overline{T})\right] \tag{8}$$

where RET_0 is the representative equilibrium temperature of the previous time step (K); Δt is time step (s); $\frac{2\pi}{\tau}$ is the angular frequency for diurnal forcing (radians s^{-1}); $\overline{T}$ is the mean surface temperature (K); and C_T is the coefficient weighted by the volumetric heat capacity of soil and canopy:

$$C_T = 1/\left(\frac{1 - f_v}{C_g} + \frac{f_v}{C_v}\right) \tag{9}$$

where C_g is the soil heat capacity (MJ m^{-3} K^{-1}) and C_v is the canopy heat capacity (MJ m^{-3} K^{-1}).

3. **Sensible heat flux (H)**

H represents heat energy transferred between the surface and air when their temperatures are different, which is the weighted average of the sensible heat flux of bare soil and the canopy:

$$H = (1 - f_v)H_s + f_v H_c \tag{10}$$

where H_s and H_c are the sensible heat flux of bare soil and the canopy (W m^{-2}), respectively, which are parameterized as:

$$H_s = \frac{\rho_a c_p}{r_{abs}}(RET - T_a) \tag{11}$$

$$H_c = \frac{\rho_a c_p}{r_a}(RET - T_a) \tag{12}$$

where ρ_a is air density (kg m^{-3}); c_p is the specific heat capacity of air (MJ kg^{-1} K^{-1}); T_a is air temperature (K); r_{abs} and r_a are the aerodynamic resistances for bare soil and canopy (s m^{-1}), respectively.

The aerodynamic resistance determines the transfer of heat and water vapor from evapotranspiration surface into the air at reference height. For the canopy component, r_a is evaluated according to Thom (1972) as:

$$r_a = \frac{[\ln(\frac{z_m - d}{z_{om}}) - \Psi_m(\frac{z_m - d}{L})][\ln(\frac{z_h - d}{z_{oh}}) - \Psi_h(\frac{z_h - d}{L})]}{k^2 u} \tag{13}$$

where z_m and z_h are the reference heights where wind and humidity are measured (m); d is the zero plane displacement height (m); z_{om} and z_{oh} are the roughness length governing the transfer of momentum and heat, respectively (m); Ψ_m and Ψ_h are atmospheric stability correction factors for momentum and heat (-), respectively; L is the Obukhov length (m); k is the Von Karman constant; and u is wind speed (m s^{-1}).

In this paper, we estimated d, z_{om} and z_{oh} by empirical functions based on canopy height h (m) (Allen et al., 1998) :

$$d = 0.666h \tag{14}$$

$$z_{om} = 0.123h \tag{15}$$

$$z_{oh} = 0.1 z_{om} \tag{16}$$

The aerodynamic resistance for bare soil r_{abs} can be determined in the same way as r_a using Eq. (13), but with different roughness length for bare soil. In this paper, we assumed 0.01 m and 0.001 m for z_{om} and z_{oh}, respectively.

4. **Latent heat flux (LE)**

LE is the energy used for the phase change of water, which is directly related to ET. It is also the weighted average of the latent heat flux of bare soil and the canopy:

$$LE = (1 - f_v)LE_s + f_v LE_c \tag{17}$$

where LE_s and LE_c are the latent heat fluxes of bare soil and the canopy (W m^{-2}), respectively, which are parameterized following Corbari et al. (2011) as:

$$LE_s = \frac{\rho_a c_p}{\gamma(r_{abs} + r_s)}(e^* - e_a) \tag{18}$$

$$LE_c = \frac{\rho_a c_p}{\gamma(r_a + r_c)}(e^* - e_a) \tag{19}$$

where γ is the psychometric constant (Pa $°C^{-1}$); r_s and r_c are resistances for bare soil and the canopy (s m^{-1}), respectively; e^* is the saturated vapor pressure of the evapotranspiration surface (Pa); and e_a is the vapor pressure of air (Pa). In particular, e^* is also related to RET:

$$e^* = 6.11 \times 10^{\frac{7.5 RET_c}{237.3 + RET_c}} \tag{20}$$

where RET_c is RET expressed in degree Celsius ($°C$)

In this paper, we parameterized r_s and r_c following the work of Corbari et al. (2011) and Yan et al. (2012), owing to the similar soil water routines of the XAJ model and models reported by these authors.

$$r_s = 3.5 \left(\frac{\theta_{sat}}{\theta}\right)^{2.3} + 33.5 \tag{21}$$

$$r_c = \frac{1}{R_h} \frac{r_{s\,min}}{LAI} \frac{\theta_{fc} - \theta_{wp}}{\theta - \theta_{wp}} \tag{22}$$

where θ_s is saturated soil moisture (-); θ is soil moisture (-); $r_{s\ min}$ is minimum stomatal resistance of canopy (s m^{-1}); R_h is relative humidity (-); and θ_{fc} and θ_{wp} are field capacity and wilting point (-), respectively.

As is summarized in Section 1, there are several approaches to derive latent heat flux from the energy balance. In this paper, we adopted the approach proposed by Corbari et al. (2011) where the energy balance is solved by determining RET,
5 which is theoretically the LST that closes the balance. Given that the energy storage term (ΔS) is often negligible at the basin scale (Corbari et al., 2011) and the remaining energy budget components in Eq. (4) are all related to RET, we employed Newton-Raphson iterative method to solve RET that can close the energy balance. As reported by Corbari et al. (2011), the Newton-Raphson method is an efficient way to solve the energy balance under different hydro-meteorological conditions. The actual LE is then solved based on the resulting RET using Eq. (17) through Eq. (22).

10 ### 2.2.1 XAJ-EB: the XAJ Model Improved by Coupling Mass-Energy Balance

The mass (Eq. 1) and energy balance (Eq. 4) is coupled through ET and W. ET is derived from LE in the energy balance as:

$$ET = \frac{LE}{\lambda \rho_w} \tag{23}$$

where λ is the latent heat of vaporization (MJ kg^{-1}); and ρ_w is the density of water (kg m^{-3}).

Different from many models that simply link mass and energy balance, an iterative algorithm is employed here to ensure
15 the fully coupling between mass and energy balance. More specifically, for a given time step, based on W of the previous time step, the energy balance calculates ET and transfers it to the mass balance to update W. The updated W is transferred back to the energy balance to calculate ET until the coupled mass-energy balance is achieved, i.e. difference in W from the last two iterations is below a pre-defined threshold (0.01 in this paper).

In order to couple the energy balance to the XAJ model, we changed the basic computational unit for runoff yield, from
20 an elementary area to a grid cell. The computational unit of the energy balance scheme is grid because all inputs to it are grid-based, which is different from that of the XAJ model. We adopted the "Grid-XAJ" concept that also employs the grid as a computational unit (Li et al., 2007; Yao et al., 2009). Here, we used a grid to compute runoff yield only, rather than all processes, because runoff separation and routing are isolated from runoff yield and do not affect the mass balance of the grid.

The improved XAJ model, i.e. XAJ-EB introduces atmospheric forcing and remote sensing data as input and calculates
25 runoff, evapotranspiration and soil water simultaneously using a grid cell based on the mass-energy balance. Runoff yield calculated for grid cells are aggregated to an elementary area for routing simulation.

By coupling the energy balance scheme, XAJ-EB is able to calculate ET based on meteorological and remote sensing data, providing ET estimation at high spatial and temporal resolution, which successfully overcomes the defects of original ET scheme of the XAJ model. More importantly, as a key variable of the energy balance solution, RET represents the equilibrium
30 temperature of the land surface that controls the entire mass-energy balance. RET is comparable to land surface temperature (LST) retrieved from remotely-sensed imagines (Corbari et al., 2011), which serves as a new constraint of the XAJ model besides runoff.

3 Evaluation of the XAJ-EB Model

3.1 Study Area

We selected a gauged catchment, namely the LuShui river catchment (LS) to test the XAJ-EB model. It is situated in the the middle reaches of Yangtze River (Chang Jiang) Basin and is controlled by the ChongYang hydrological site (Figure 3). LS covers an area of 2250 km^2, ranging from 29.08N to 29.83N and 113.67E to 114.17E. Annual precipitation, pan evaporation and runoff depth of LS are 1550 mm, 1200 mm and 753.3 mm, respectively (Cheng et al., 2013). The study area is mainly characterized by mountain and hill terrain which covers more than 90 % the total area, with a mean elevation of 258 m. According to MODIS-based land cover climatology data (Broxton et al., 2014), the major land cover types of this area are crop land and mixed forests. There are 8 precipitation sites and 1 hydrological site within the catchment, operated by the Bureau of Hydrology, Yangtze River Water Resources Commission.

Figure 3 here

3.2 Data

3.2.1 Digital Elevation Model (DEM)

We mainly relied on digital elevation model (DEM) to delineate the sub-catchments and elementary areas (the basic computational unit of the XAJ model, see Section 2.1 for details). The DEM dataset employed in this paper was ASTER (Advanced Spaceborne Thermal Emission and Reflection Radiometer) DEM Version 2, released in October, 2011 by the U.S. National Aeronautics and Space Administration (NASA) and Japan's Ministry of Economy, Trade, and Industry (METI). The spatial resolution of ASTER DEM is 1″ (approximately 30 m in the study area). DEM data were downloaded from http://dx.doi.org/10.5067/ASTER/ASTGTM.002 and extracted based on the boundary of LS. To match the spatial scale of the model (see Section 3.3 for details), we further resampled the DEM to the spatial resolution of 1 km using majority resampling technique.

3.2.2 Land Cover and Soil Data

Land cover and soil data were used to determine several land cover or soil-dependent parameters (e.g. minimal stomatal resistance and soil tension water capacity) of the model.

The land cover dataset we chose was 0.5 km MODIS-based Global Land Cover Climatology developed by Broxton et al. (2014) based on 10 years (2001-2010) of the MODIS land cover (MCD12Q1, Collection 5.1) product. The dataset classified the land surface into 17 different land cover types, avoiding the unrealistic land cover change as observed by the original MCD12Q1 product. The land cover dataset is available online at http://landcover.usgs.gov/global_climatology.php. Similar to the DEM data, we resampled the land cover data into 1 km spatial resolution using majority resampling technique.

We mainly used 2 types of soil data properties for this study, i.e. soil physical properties (e.g. field capacity) which were obtained from a data set developed by Dai et al. (2013), and soil thickness obtained from a data set developed by Pelletier

et al. (2015). The former data set, namely the "China data set of soil properties", was developed mainly for land surface modeling and includes various soil hydraulic parameters derived from soil physical and chemical properties using pedotransfer functions (Dai et al., 2013). The spatial resolution of this dataset is 30″ (approximately 1 km in the study area) and the vertical variation of the soil properties is documented for 7 layers to a depth of 1.38 m. The soil properties data were retrieved from http://globalchange.bnu.edu.cn/research/soil3. The latter data set, namely the "gridded global data set of soil, immobile regolith, and sedimentary deposit thicknesses", documents the estimation of the thickness of the permeable layers above the bedrock (Pelletier et al., 2015), which can be regarded as soil depth defined by the XAJ model. This dataset was retrieved from http://dx.doi.org/10.3334/ORNLDAAC/1304, and it has the same spatial resolution as the China data set of soil properties at 30″.

3.2.3   Remote Sensing Data

Variables retrieved from remote sensing data were used to drive (e.g. leaf area index (LAI) and Albedo) or validate the model (e.g. land surface temperature (LST)). We adopted various Moderate Resolution Imaging Spectroradiometer (MODIS) products to provide spatial estimations of LAI, Albedo and LST; detailed information on these variables, including product name and spatial and temporal resolution can be found in Table 2. All remote sensing data were download from http://reverb.echo.nasa.gov/ for the period between year 2004 and 2007. The Albedo dataset was resampled to a 1 km spatial resolution.

Table 2 here

3.2.4   Meteorological and Hydrological Data

The meteorological forcing data we employed included precipitation, downward short wave radiation, downward long wave radiation, wind speed, air temperature, air pressure and specific humidity from 2004 to 2007. Precipitation data from 8 rain gauges were collected by the Bureau of Hydrology, Yangtze River Water Resources Commission. All other forcing data were retrieved from the China Meteorological Forcing Dataset (CMFD) (He and Yang, 2011) which was produced by merging a variety of data sources (Chen et al., 2011; Leng et al., 2015).The spatial and temporal resolutions of this dataset are $0.1°$ (approximately 10 km in the study area) and 3 hours, respectively. The dataset was downloaded from http://westdc.westgis.ac.cn/. Runoff and pan evaporation data of the ChongYang hydrological station for the same period were also collected by the Bureau of Hydrology.

3.3   Model Setup

In consideration of the catchment characteristics as well as data availability, we defined the dimension of the computational grid as 1 km $\times$ 1 km, resulting in 72 columns $\times$ 60 rows that covered the study area. All other datasets were resampled to 1 km $\times$ 1 km resolution. The temporal resolution of the model is 3 h, the same as the meteorological forcing data.

The estimation of areal mean precipitation in the computational grid is crucial for the accurate hydrological modeling. Several approaches existed for spatially interpolating the precipitation from gauges, however, their performances and uncertainties

depend on certain conditions including the pattern of precipitation, the characteristic of catchment, and the locations of gauges (Ball and Luk, 1998; Di Piazza et al., 2011; Zhang and Srinivasan, 2009). It's difficult to evaluate the performance of different interpolation approaches in LS since the true areal precipitation is theoretically not available. In this paper, the conventional Thiessen polygon approach, the one intensively used in the XAJ model, was employed to derive the spatially-distributed pre-
5   cipitation from 8 gauges. To make the precipitation inputs of XAJ-EB comparable to those of XAJ, the precipitation of gauges are interpolated to grids by following steps:

(1) Thiessen polygons were generated according to the geographic locations of gauges;

(2) Thiessen polygons were overlaid with element areas, and the precipitation of ith element area (P_i) was weighted by Thiessen polygons that intersected with it (the precipitation of green-filled element area in Figure 4 was determined by Thiessen
10   polygons 1, 3, 4 and 5, taking their area as weight);

(3) Grids belongs to the same element area i were assigned the same precipitation P_i.

As seen from Eq. 4 through Eq. 22, a range of parameters/variables is needed for the energy balance scheme. Each grid was assigned a set of time-independent parameters including soil physical properties (e.g. θ_{fc}) , vegetation properties (e.g. $r_{s\ min}$) based on soil and vegetation type. Other time-dependent variables were obtained either from remote sensing data (e.g. LAI) or
15   model simulated states (e.g. θ).

3.4   Calibration and Validation of the XAJ Model

As listed in Table 1, several parameters have to be estimated before applying the XAJ model, among which tension water capacity WM has physical definition that can be estimated from the soil proprieties for each grid:

$$WM = (\theta_{fc} - \theta_{wp}) \times SD \tag{24}$$

20   where SD is soil depth (mm). All three soil proprieties can be retrieved from soil dataset described above.

For parameters other than WM, two years of data (2004 and 2005) was chose to perform a calibration against observed runoff data using the original XAJ model, which calculates ET using measured pan evaporation.

We first introduced a model-independent parameter estimation tool, namely PEST (Doherty et al., 1994) to provide an optimized combination of parameters. PEST is based on the Gauss-Marquardt Levenberg (GML) algorithm (Marquardt, 1963)
25   and has been widely applied in calibrating hydrological models. The initial values as well as the optimization limits of the parameters were set according to Zhao (1984). After the automatic calibration, we used the traditional trial and error method to adjust some parameters based on our experience in calibrating the XAJ model. This is because the algorithm implemented by PEST tries to fit the complete time-series of runoff observations, regardless of high flows or low flows, while the flood events are the major concerns of real-time flood forecasting. As such, the trial and error method was applied to improve the
30   simulations of high flows based on parameters optimized by PEST.

The metrics adopted to evaluate the model performance are the root-mean-square error (RMSE), Nash-Sutcliffe model efficiency coefficient (NSE) and relative error of total runoff volume (bias):

$$RMSE = \sqrt{\frac{1}{n}\sum_{i=1}^{n}(Q_{obs,i} - Q_{sim,i})^2} \tag{25}$$

$$NSE = 1 - \frac{\sum_{i=1}^{n}(Q_{obs,i} - Q_{sim,i})^2}{\sum_{i=1}^{n}(Q_{obs,i} - \overline{Q}_{obs})^2} \tag{26}$$

5 $$bias = \frac{V_{sim} - V_{obs}}{V_{obs}} \tag{27}$$

$$V_{sim} = \sum_{i=1}^{n-1}\left(\frac{Q_{sim,1} + Q_{sim,i+1}}{2}\right)\Delta t_i \tag{28}$$

$$V_{obs} = \sum_{i=1}^{n-1}\left(\frac{Q_{obs,1} + Q_{obs,i+1}}{2}\right)\Delta t_i \tag{29}$$

where $Q_{obs,i}$ and $Q_{sim,i}$ are observed and modeled discharge (m^3 s^{-1}) at time step i, respectively; n is total time step; and Δt_i is the interval between time step i and $i+1$ (s).

10   Table 1 summaries the optimized parameter values while Figure 5a shows comparison between XAJ-modeled and observed runoff during the calibration period. The XAJ model reproduced both the variation and amplitude of flood events with RMSE, NSE and bias values of 37.96 m^3 s^{-1}, 0.70 and -0.09 %, respectively, which indicates the good performance of the model and the efficiency of our calibration strategy. One important objective of the calibration process was to control the overall water balance (-0.09%) by adjusting KC based on pan evaporation, because the model performance is sensitive to the accuracy and

15   representativeness of the pan evaporation observations.

To validate the model, we ran the model for another two years (2006 and 2007) with these calibrated parameters. Figure 5b presents the validation results which shows the good agreement between XAJ-modeled and observed runoff, although the XAJ model slightly overestimated the total runoff volume by 2.18%, the RMSE and NSE were even better than the values obtained during the calibration period, further confirming the fitness and robustness of the parameters we calibrated.

20   **Figure 5 here**

3.5   Validation of XAJ-EB Against Runoff

Given that the mass balance of the XAJ model remained unchanged, we used the calibrated parameters directly to run the XAJ-EB model for the whole period between 2004 and 2007. For this simulation using XAJ-EB, the coefficient KC was eliminated since the ET was simulated directly using the mass-energy balance scheme. Figure 6 shows the comparison between XAJ-EB

25   modeled and observed runoff. The overall RMSE, NSE and bias ewre 26.09 m^3 s^{-1}, 0.77 and -0.53%, respectively. The overall performance of the runoff simulation by XAJ-EB is comparable to that of the original XAJ model.

Figure 6 here

3.6 Validation of XAJ-EB Against MODIS LST

The RET simulated by XAJ-EB is theoretically the LST that closes the energy balance, which is comparable to the LST retrieved from remote-sensing data, providing another variable for model calibration and validation. Among various LST products released, the MODIS LST products have been widely used owing to high accuracy (Corbari et al., 2011, 2014b; Wan et al., 2004). The dataset we used in this paper is the MOD11A1 daytime LST product. Although it is available daily at a 1 km spatial resolution, some images are affected by cloud, resulting in a high number of missing values. In order to better validate the LST simulation, we examined each image for the whole simulation period and chose 107 images with a maximum of 30% missing values.

We first performed grid-by-grid comparison using the sampling XAJ-EB modeled LST according to MODIS LST data availability, the fitness was evaluated by coefficient of determination (R^2):

$$R^2 = \left[\frac{n(\sum_{i=1}^{n} LST_{sim,i}LST_{obs,i}) - \sum_{i=1}^{n} LST_{sim,i} \sum_{i=1}^{n} LST_{obs,i}}{\sqrt{[n(\sum_{i=1}^{n} LST_{sim,i}^2) - (\sum_{i=1}^{n} LST_{sim,i})^2][n(\sum_{i=1}^{n} LST_{obs,i}^2) - (\sum_{i=1}^{n} LST_{obs,i})^2]}} \right]^2 \tag{30}$$

where LST_{sim_i} and LST_{obs_i} are XAJ-EB-modeled and MODI-retrieved LST (K), respectively at time step i; and n is the total LST data to be evaluated.

Figure 7a shows the scatter plot between the XAJ-EB modeled and MODIS retrieved grid LST for all 107 MODIS images we chose; the resulting R^2 value reached reaches 0.91, indicating the good agreement between the two variables. We also plotted the catchment average LST (Figure 7b), from which we can clearly see that most LST points are distributed along the 1:1 line with small deviation. Figure 7 indicates that XAJ-EB is capable of accurately simulating LST under various hydrometeorological and underlying surface conditions.

We also plotted the time series of XAJ-EB-modeled catchment-average LST against MODIS-retrieved catchment-average LST (Figure 8), and calculated the corresponding RMSE and NSE values as 2.25 K and 0.89, respectively. The results are acceptable since the overall accuracy of the MODIS LST product is reported to be ±1 K (Kalma et al., 2008), which further confirm the fit between XAJ-EB modeled and MODIS retrieved LST.

Figure 7 here

Figure 8 here

3.7 Validation of XAJ-EB Against MODIS ET

There were no direct ET measurements in the LS catchment due to the lack of eddy flux towers. Consequently, to evaluate the ET simulation from XAJ-EB, we adopted the MODIS ET(MOD16A2) product as the reference. Different from the MODIS LST product, MODIS ET is based on the P-M equation using various MODIS products(Mu et al., 2007, 2011). Although many studies have confirmed the overall accuracy of the product, the specific accuracy over some regions cannot always be

guaranteed due to the algorithm itself as well as land surface characteristics (Corbari et al., 2014b; Mu et al., 2007, 2011; Ramoelo et al., 2014; Roux et al., 2013).

Figure 9 shows the catchment average of XAJ-EB modeled and MODIS-estimated 8-day ET, we also included the XAJ-modeled ET here for comparison. Total MODIS-estimated ET for this period is 3234.8 mm, higher than the 2655.7 mm from XAJ-EB and 2393.4 mm from XAJ. However, the cumulative observed precipitation and runoff values for the whole study period were 4609.0 mm and 2193.3 mm, respectively, from which we can roughly estimate the cumulative ET for the same period as 2416.7 mm if we assume total precipitation can be balanced by ET and runoff over such a long period. Corbari et al. (2014b) reported an overestimate of MODIS ET for the Yangtze River basin, which is in accordance with our results as shown in Figure 9, i.e. MODIS ET is higher than ET from both models. Although there is bias in the total ET estimation, XAJ-EB-modeled ET had an R^2 value of 0.70, higher than that of the XAJ modeled ET (0.50), which means the variation in ET from XAJ-EB was close to MODIS-estimated ET.

Figure 9 here

4　Discussion

4.1　Advantages of XAJ-EB over XAJ

In this paper, the original XAJ model was improved by coupling the mass-energy balance scheme. Validations using both ground measured runoff and remotely-sensed LST have proved the performance of XAJ-EB. Compared with the original XAJ model, there are some obvious advantages of the XAJ-EB model that overcome the several defects as we reported in Section 1. First the model is capable of providing more reliable ET at high spatial and temporal resolution based on meteorological forcing and remotely sensed data, which may influence the soil moisture and further influence the runoff simulation. During 2007, we can see from Figure 10b that the most significant difference occurred during the dry season when there was little precipitation, and the low SMC from XAJ-EB before the two largest flood events reduced the flood peak, which was closer to the observations (Figure 10a).

Figure 10 here

Another advantage is that XAJ-EB is more suitable for use in ungauged basins, where either measured pan evaporation or runoff data are unavailable. This is because XAJ-EB simulates ET based on meteorological forgings and remotely sensed data, rather than measured pan evaporation used by XAJ. Moreover, LST is a crucial parameter controlling the mass-energy balance, which reflects the interactions among different processes (Wang et al., 2009). Moreover, LST is also an indicator of SMC variation (Corbari et al., 2011; Sandholt et al., 2002). Therefore, the model-simulated LST provides an alternative way to calibrate and validate the spatially-distributed parameters, especially when observed runoff data are unavailable. In fact, some efforts have been made to exploit the LST for hydrological modeling (Corbari and Mancini, 2014; Corbari et al., 2014a; Silvestro et al., 2013; Wang et al., 2009), and these studies have demonstrated the possibility of using LST as a supplement to traditional runoff data.

14

Finally, the XAJ model is not for flood foresting only, it has been used for investigating the effects of climate (Peng and Xu, 2010) or land cover (Tian et al., 2013; Qu et al., 2011) change on stream flow; identifying the drought events (Duan and Mei, 2014) and examining the variability of SMC memory for wet and dry basins (Rahman et al., 2015). Such studies can benefit from reliable ET and SMC simulation. By explicitly take into consideration meteorological forcing, land cover and vegetation characteristics, XAJ-EB is more suitable than XAJ for the study of hydrological responses under changing climate/land cover, which may help to extend the applications of original XAJ model.

4.2 Applicability of simplified energy balance of XAJ-EB

As we mentioned in Section 1, the energy balance scheme developed for the XAJ model is physically-based with proper structures that are suitable for real-time flood forecasting operations. Consequently, we used certain generalizations and simplications, especially for LST, we adopted a lumped RET to represent the integrated LST for the land surface. In contrast, some LSMs involve more sophisticated schemes, e.g. Noah-MP LSM (Niu et al., 2011) introduced 3 different LSTs: $T_{g,b}$ for temperature of bare ground fraction, $T_{g,v}$ for temperature of the vegetated fraction and T_v for canopy surface temperature.

To further investigate the applicability of XAJ-EB, we ran Noah-MP with the same dataset we used for XAJ-EB but excluded precipitation. Because Noah-MP requires grid precipitation input, we used the CMFD precipitation field rather than the gauge-measured value. Figure 11 presents the comparison of daily LST and latent heat flux from XAJ-EB with those from Noah-MP.

LST from Noah-MP was estimated using the simulated upward long wave radiation which represents the integration of different land surface components within the grid (see Niu et al., 2011, for details). Figure 11a shows a generally good agreement between the XAJ-EB and Noah-MP simulated LST, with RMSE, NSE and bias values as 1.68 K, 0.97 and -0.20%. Such good agreement indicates that, comparing with Noah-MP with multiple LSTs, the energy balance scheme of XAJ-EB is able to produce reliable LST with only one lumped temperature.

As for the latent heat flux, although the overall bias was small (-2.53 %), low NSE (0.53) indicates there is an inconsistency in inconsistence of the ET time series. This is partly due to the different precipitation fields we used for the 2 models, which had an NSE of only 0.51 (Figure 11c). By comparing Figure 11b with Figure 11c we found that a larger bias of ET generally corresponds to a larger bias in precipitation.

<center>**Figure 11 here**</center>

In addition to the simplification of the energy balance scheme, XAJ-EB also makes use of various remote sensing products (i.e. LAI, Albedo, etc.) to eliminate the processes that have little effects on flood forecasting (e.g. vegetation dynamics), only retaining the essential processes that related to ET and runoff simulation, which help to reduce both the complexity of the model and number of parameters need calibrated.

4.3 Calibration strategy of the model

Calibration is necessary for hydrological models, even for the physically-based models (Singh and Bárdossy, 2012). There has been the concern regarding the selection of runoff observations for calibration. In general, runoff data including both dry and

<center>15</center>

wet conditions is required to represent the various characteristics of the catchment, from which the stable and robust parameter values can be obtained (PERRIN et al., 2007; Razavi and Tolson, 2013; Singh and Bárdossy, 2012). However, considering the data availability, researchers have been studying the calibration strategies using runoff observations of short period (e.g. Kim and Kaluarachchi, 2009; Sun et al., 2016; Wang et al., 2017). Although specific results differ depending on the catchments as well as the models adopted, they all found that high-flow periods exert greater influence on model calibration, which implies that the hydrological models can be calibrated against high flows, which are more important for real-time forecasting.

To validate the energy balance scheme as well as the XAJ-EB model developed in this paper, a two-step calibration of the XAJ model was applied (Section 3.4). The first step was to calibrate the parameters using PEST based on the complete time-series of runoff observations. This is because the calibration of parameter KC requires complete runoff observations of several years to ensure that the accumulated simulated runoff was close to the corresponding observed value (Zhao, 1992); and (2) the validation of LST and ET from XAJ-EB also requires accurate mass balance simulations all over the year, covering flood and non-flood periods, to better evaluate the performance of the model under various hydrometeorological conditions. Then for the second step, the trial and error method was applied to adjust the resulting optimized parameters, mainly according to the high flows of flood events. Such straightforward but effective calibration strategy stroked a balance between the representativeness of the runoff data and the importance of large flood events, providing the reliable baseline to validate the XAJ-EB model in this study. However, a more rigorous quantification of the uncertainties in parameters calibration is need for the XAJ and XAJ-EB model in subsequent studies.

5 Conclusion

In this paper, an energy balance based scheme suitable for the XAJ model was developed by explicitly taking account of bare soil and the canopy using a "patch approach". Different energy fluxes for bare soil and the canopy respectively were parameterized. The energy balance was simulated by determining RET, which is theoretically the LST that closes the balance. The energy balance scheme was then fully coupled to the mass mass balance scheme of the XAJ model. The improved model, XAJ-EB estimates the actual ET and runoff yield through a mass-energy balance approach using various meteorological and remotely sensed data.

Taking the LS catchment as the study area, we calibrated and validated the original XAJ model and used the same optimized parameters to evaluate the performance of the XAJ-EB model. With respect to the runoff simulation for the period between 2004 and 2007, the XAJ-EB model had RMSE, NSE and bias values of 26.09 $\mathrm{m^3\,s^{-1}}$, 0.77 and -0.53%, respectively. The results well matched with the observed runoff, which was also comparable to the original XAJ model. In addition to runoff, XAJ-EB is also capable of simulating the dynamics of LST with R^2, RMSE and NSE values of 0.93, 2.25 K and 0.89, respectively compared with MODIS-retrieved catchment average LST. The good match between modeled and remotely-sensed LST implies that the XAJ-EB model is able to reproduce the mass-energy balance processes since LST reflects the interactions among various processes. Moreover, with LST as an output, XAJ-EB adds a new constraint and offers a potentially new approach for model calibration and validation, especially when runoff data are unavailable.

The mass-energy balance scheme developed in this paper is comparable to the sophisticated LSM Noah-MP model in terms of LST and latent heat flux modeling, which overcomes several defects of the original XAJ model that simulates actual ET using pan evaporation measurements. The inter-comparison between XAJ-EB and XAJ shows that the improvement of ET estimation helps to improve the runoff simulation, especially the runoff peak which is the major concern of real-time flood forecasting. Moreover, by explicitly take consideration of different atmospheric and underlying surface conditions, XAJ-EB is more suitable than XAJ for the study of hydrological responses under changing climate/land cover, which extend the applications of the original XAJ model.

References

Allen, R. G., Pereira, L. S., Raes, D., Smith, M., et al.: Crop evapotranspiration-Guidelines for computing crop water requirements-FAO Irrigation and drainage paper 56, FAO, Rome, 300, D05 109, 1998.

Ball, J. E. and Luk, K. C.: Modeling Spatial Variability of Rainfall over a Catchment, J. Hydrol. Eng., 3, 122–130, doi:10.1061/(ASCE)1084-0699(1998)3:2(122), http://ascelibrary.org/doi/10.1061/(ASCE)1084-0699(1998)3:2(122), 1998.

Bergström, S., Singh, V., et al.: Computer models of watershed hydrology, chap. The HBV model, pp. 443–476, Water Resources Publications, 1995.

Berthet, L., Andréassian, V., Perrin, C., and Javelle, P.: How crucial is it to account for the antecedent moisture conditions in flood forecasting? Comparison of event-based and continuous approaches on 178 catchments, Hydrology and Earth System Sciences Discussions, pp. p–819, 2009.

Bhumralkar, C.: Numerical experiments on the computation of ground surface temperature in an atmospheric general circulation model, doi:10.1175/1520-0450(1975)014<1246:NEOTCO>2.0.CO;2, http://journals.ametsoc.org/doi/abs/10.1175/1520-0450(1975)014{\T1\textless}1246:NEOTCO{\T1\textgreater}2.0.CO;2, 1975.

Blackadar, A. K.: Modeling the Nocturnal Boundary Layer, in: Prepr. Third Symp. Atmos. Turbul. Diffus. Air, pp. 46–49, 1976.

Blöschl, G., Reszler, C., and Komma, J.: A spatially distributed flash flood forecasting model, Environmental Modelling & Software, 23, 464–478, 2008.

Brocca, L., Melone, F., Moramarco, T., and Singh, V.: Assimilation of observed soil moisture data in storm rainfall-runoff modeling, Journal of Hydrologic Engineering, 14, 153–165, 2009.

Broxton, P. D., Zeng, X., Sulla-Menashe, D., and Troch, P. A.: A global land cover climatology using MODIS data, Journal of Applied Meteorology and Climatology, 53, 1593–1605, 2014.

Burnash, R., Ferral, R., McGuire, R., McGuire, R., and Center, U. S. J. F.-S. R. F.: A Generalized Streamflow Simulation System: Conceptual Modeling for Digital Computers, U.S. Department of Commerce, National Weather Service, and State of California, Department of Water Resources, https://books.google.com.hk/books?id=aQJDAAAAIAAJ, 1973.

Cellier, P., Richard, G., and Robin, P.: Partition of sensible heat fluxes into bare soil and the atmosphere, Agric. For. Meteorol., 82, 245–265, doi:http://dx.doi.org/10.1016/0168-1923(95)02328-3, http://www.sciencedirect.com/science/article/pii/0168192395023283, 1996.

Chen, Y., Yang, K., He, J., Qin, J., Shi, J., Du, J., and He, Q.: Improving land surface temperature modeling for dry land of China, Journal of Geophysical Research: Atmospheres, 116, 2011.

Chen, Y., Li, J., and Xu, H.: Improving flood forecasting capability of physically based distributed hydrological models by parameter optimization, Hydrology and Earth System Sciences, 20, 375–392, doi:10.5194/hess-20-375-2016, http://www.hydrol-earth-syst-sci.net/20/375/2016/, 2016.

Cheng, M., Chengshou, D. U., and Zheng, G.: Analysis on hydrologic characteristics of Lushui River Basin (in Chinese), Yangtze River, 2013.

Cloke, H. and Pappenberger, F.: Ensemble flood forecasting: a review, Journal of Hydrology, 375, 613–626, 2009.

Corbari, C. and Mancini, M.: Calibration and validation of a distributed energy–water balance model using satellite data of land surface temperature and ground discharge measurements, Journal of Hydrometeorology, 15, 376–392, 2014.

Corbari, C., Ravazzani, G., and Mancini, M.: A distributed thermodynamic model for energy and mass balance computation: FEST–EWB, Hydrological Processes, 25, 1443–1452, 2011.
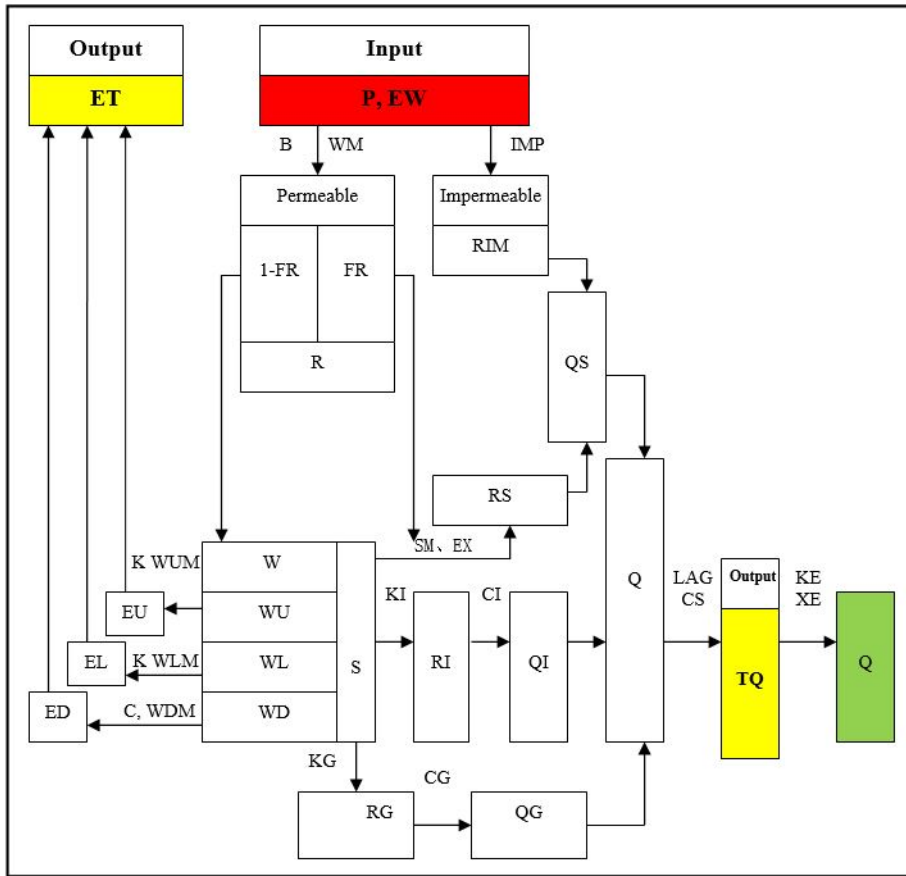
Corbari, C., Sobrino, J. A., Mancini, M., and Hidalgo, V.: Mass and energy flux estimates at different spatial resolutions in a heterogeneous area through a distributed energy–water balance model and remote-sensing data, International journal of remote sensing, 34, 3208–3230, 2013.

Corbari, C., Mancini, M., Li, J., and Su, Z.: Can satellite land surface temperature data be used similarly to river discharge measurements for distributed hydrological model calibration?, Hydrol. Sci. J., 60, 202–217, doi:10.1080/02626667.2013.866709, http://www.tandfonline.com/doi/abs/10.1080/02626667.2013.866709, 2014a.

Corbari, C., Mancini, M., Su, Z., and Li, J.: Evapotranspiration estimate from water balance closure using satellite data for the Upper Yangtze River basin, Hydrol. Res., 45, 603–614, doi:10.2166/nh.2013.016, 2014b.

Dai, Y., Shangguan, W., Duan, Q., Liu, B., Fu, S., and Niu, G.: Development of a China dataset of soil hydraulic parameters using pedotransfer functions for land surface modeling, Journal of Hydrometeorology, 14, 869–887, 2013.

Deardorff, J. W.: Efficient prediction of ground surface temperature and moisture, with inclusion of a layer of vegetation, J. Geophys. Res., 83, 1889, doi:10.1029/JC083iC04p01889, http://doi.wiley.com/10.1029/JC083iC04p01889, 1978.

Di Piazza, A., Conti, F. L., Noto, L., Viola, F., and La Loggia, G.: Comparative analysis of different techniques for spatial interpolation of rainfall data to create a serially complete monthly time series of precipitation for Sicily, Italy, Int. J. Appl. Earth Obs. Geoinf., 13, 396–408, doi:10.1016/j.jag.2011.01.005, http://linkinghub.elsevier.com/retrieve/pii/S0303243411000225, 2011.

Doherty, J., Brebber, L., and Whyte, P.: PEST: Model-independent parameter estimation, Watermark Computing, Corinda, Australia, 122, 1994.

Duan, K. and Mei, Y.: Comparison of meteorological, hydrological and agricultural drought responses to climate change and uncertainty assessment, Water resources management, 28, 5039–5054, 2014.

Hapuarachchi, H. A. P., Wang, Q. J., and Pagano, T. C.: A review of advances in flash flood forecasting, Hydrological Processes, 25, 2771–2784, doi:10.1002/hyp.8040, http://dx.doi.org/10.1002/hyp.8040, 2011.

He, J. and Yang, K.: China Meteorological Forcing Dataset, Cold and Arid Regions Science Data Center at Lanzhou, 2011.

Huza, J., Teuling, A. J., Braud, I., Grazioli, J., Melsen, L. A., Nord, G., Raupach, T. H., and Uijlenhoet, R.: Precipitation, soil moisture and runoff variability in a small river catchment (Ardèche, France) during HyMeX Special Observation Period 1, Journal of Hydrology, 516, 330–342, 2014.

Idso, S., Aase, J., and Jackson, R.: Net radiation ? soil heat flux relations as influenced by soil water content variations, Boundary-Layer Meteorol., 9, 113–122, doi:10.1007/BF00232257, http://link.springer.com/10.1007/BF00232257, 1975.

Kalma, J. D., Mcvicar, T. R., and Mccabe, M. F.: Estimating Land Surface Evaporation: A Review of Methods Using Remotely Sensed Surface Temperature Data, Surveys in Geophysics, 29, 421–469, 2008.

Kampf, S. K. and Burges, S. J.: A framework for classifying and comparing distributed hillslope and catchment hydrologic models, Water Resources Research, 43, 2007.

Kim, U. and Kaluarachchi, J. J.: Hydrologic model calibration using discontinuous data: an example from the upper Blue Nile River Basin of Ethiopia, Hydrol. Process., pp. n/a–n/a, doi:10.1002/hyp.7465, http://doi.wiley.com/10.1002/hyp.7465, 2009.

Kobold, M. and Brilly, M.: The use of HBV model for flash flood forecasting, Natural Hazards and Earth System Sciences, 6, 407–417, doi:10.5194/nhess-6-407-2006, http://www.nat-hazards-earth-syst-sci.net/6/407/2006/, 2006.

Komma, J., Blöschl, G., and Reszler, C.: Soil moisture updating by Ensemble Kalman Filtering in real-time flood forecasting, Journal of Hydrology, 357, 228 – 242, doi:http://dx.doi.org/10.1016/j.jhydrol.2008.05.020, http://www.sciencedirect.com/science/article/pii/S0022169408002254, 2008.

Leng, G., Tang, Q., Huang, M., and Leung, L.-y. R.: A comparative analysis of the impacts of climate change and irrigation on land surface and subsurface hydrology in the North China Plain, Regional Environmental Change, 15, 251–263, 2015.

Lhomme, J.-P. and Chehbouni, A.: Comments on dual-source vegetation–atmosphere transfer models, Agricultural and Forest Meteorology, 94, 269–273, 1999.

5   Li, H., Zhang, Y., Chiew, F. H., and Xu, S.: Predicting runoff in ungauged catchments by using Xinanjiang model with {MODIS} leaf area index, Journal of Hydrology, 370, 155 – 162, doi:http://dx.doi.org/10.1016/j.jhydrol.2009.03.003, http://www.sciencedirect.com/science/article/pii/S0022169409001504, 2009.

Li, Z., Xin, P., and Tang, J.: Study of the Xinanjiang model parameter calibration, Journal of Hydrologic Engineering, 18, 1513–1521, 2011.

Li, Z.-J., Yao, C., and Wang, Z. H.: Development and application of grid-based Xinanjiang model (in Chinese), Journal of Hohai University,

10   35, 131–134, 2007.

Liebethal, C. and Foken, T.: Evaluation of six parameterization approaches for the ground heat flux, Theor. Appl. Climatol., 88, 43–56, doi:10.1007/s00704-005-0234-0, http://link.springer.com/10.1007/s00704-005-0234-0, 2007.

Liu, J., Chen, X., Zhang, J., and Flury, M.: Coupling the Xinanjiang model to a kinematic flow model based on digital drainage networks for flood forecasting, Hydrological Processes, 23, 1337–1348, doi:10.1002/hyp.7255, http://dx.doi.org/10.1002/hyp.7255, 2009.

15   Lu, G., Wu, Z., Wen, L., Lin, C. A., Zhang, J., and Yang, Y.: Real-time flood forecast and flood alert map over the Huaihe River Basin in China using a coupled hydro-meteorological modeling system, Science in China Series E: Technological Sciences, 51, 1049–1063, 2008.

Lu, H., Liu, T., Yang, Y., and Yao, D.: A hybrid dual-source model of estimating evapotranspiration over different ecosystems and implications for satellite-based approaches, Remote Sensing, 6, 8359–8386, 2014.

Marquardt, D. W.: An algorithm for least-squares estimation of nonlinear parameters, Journal of the society for Industrial and Applied

20   Mathematics, 11, 431–441, 1963.

Masseroni, D., Corbari, C., and Mancini, M.: Effect of the representative source area for eddy covariance measurements on energy balance closure for maize fields in the Po Valley, Italy, International Journal of Agriculture and Forestry, 1, 1–8, 2011.

McCumber, M. C. and Pielke, R. A.: Simulation of the effects of surface fluxes of heat and moisture in a mesoscale numerical model: 1. Soil layer, Journal of Geophysical Research: Oceans, 86, 9929–9938, 1981.

25   Mu, Q., Heinsch, F. A., Zhao, M., and Running, S. W.: Development of a global evapotranspiration algorithm based on MODIS and global meteorology data, Remote Sens. Environ., 111, 519–536, doi:10.1016/j.rse.2007.04.015, http://linkinghub.elsevier.com/retrieve/pii/S0034425707001903, 2007.

Mu, Q., Zhao, M., and Running, S. W.: Improvements to a MODIS global terrestrial evapotranspiration algorithm, Remote Sens. Environ., 115, 1781–1800, doi:10.1016/j.rse.2011.02.019, http://linkinghub.elsevier.com/retrieve/pii/S0034425711000691, 2011.

30   Niu, G.-Y., Yang, Z.-L., Mitchell, K. E., Chen, F., Ek, M. B., Barlage, M., Kumar, A., Manning, K., Niyogi, D., Rosero, E., et al.: The community Noah land surface model with multiparameterization options (Noah-MP): 1. Model description and evaluation with local-scale measurements, Journal of Geophysical Research: Atmospheres, 116, 2011.

Niu, G.-Y., Paniconi, C., Troch, P. A., Scott, R. L., Durcik, M., Zeng, X., Huxman, T., and Goodrich, D. C.: An integrated modelling framework of catchment-scale ecohydrological processes: 1. Model description and tests over an energy-limited watershed, Ecohydrology,

35   7, 427–439, 2014.

Overgaard, J., Rosbjerg, D., and Butts, M.: Land-surface modelling in hydrological perspective? a review, Biogeosciences, 3, 229–241, 2006.

Pelletier, J. D., Broxton, P. D., Hazenberg, P., Zeng, X., Troch, P. A., Niu, G.-Y., Williams, Z., Brunke, M. A., and Gochis, D.: A gridded global data set of soil, immobile regolith, and sedimentary deposit thicknesses for regional and global land surface modeling, Journal of Advances in Modeling Earth Systems, 2015.

Peng, D. and Xu, Z.: Simulating the Impact of climate change on streamflow in the Tarim River basin by using a modified semi-distributed monthly water balance model, Hydrological processes, 24, 209–216, 2010.

PERRIN, C., OUDIN, L., ANDREASSIAN, V., ROJAS-SERNA, C., MICHEL, C., and MATHEVET, T.: Impact of limited streamflow data on the efficiency and the parameters of rainfall—runoff models, Hydrol. Sci. J., 52, 131–151, doi:10.1623/hysj.52.1.131, http://www.tandfonline.com/doi/abs/10.1623/hysj.52.1.131, 2007.

Qu, S., Bao, W., Shi, P., Yu, Z., Li, P., Zhang, B., and Jiang, P.: Evaluation of Runoff Responses to Land Use Changes and Land Cover Changes in the Upper Huaihe River Basin, China, Journal of Hydrologic Engineering, 17, 800–806, 2011.

Rabuffetti, D., Ravazzani, G., Corbari, C., and Mancini, M.: Verification of operational Quantitative Discharge Forecast (QDF) for a regional warning system? the AMPHORE case studies in the upper Po River, Natural Hazards and Earth System Science, 8, 161–173, 2008.

Rahman, M. M., Lu, M., and Kyi, K. H.: Variability of soil moisture memory for wet and dry basins, Journal of Hydrology, 523, 107 – 118, doi:http://dx.doi.org/10.1016/j.jhydrol.2015.01.033, http://www.sciencedirect.com/science/article/pii/S0022169415000505, 2015.

Ramoelo, A., Majozi, N., Mathieu, R., Jovanovic, N., Nickless, A., and Dzikiti, S.: Validation of Global Evapotranspiration Product (MOD16) using Flux Tower Data in the African Savanna, South Africa, Remote Sens., 6, 7406–7423, doi:10.3390/rs6087406, http://www.mdpi.com/2072-4292/6/8/7406/htm, 2014.

Razavi, S. and Tolson, B. A.: An efficient framework for hydrologic model calibration on long data periods, Water Resour. Res., 49, 8418–8431, doi:10.1002/2012WR013442, http://doi.wiley.com/10.1002/2012WR013442, 2013.

Roux, E., Paz, a. R., Aragao, L. E. O. C., Mu, Q., Malhi, Y., Collischonn, W., Rocha, H. R., Running, S. W., Ruhoff, a. L., Paz, a. R., Aragao, L. E. O. C., Mu, Q., Malhi, Y., Collischonn, W., Rocha, H. R., and Running, S. W.: Assessment of the MODIS global evapotranspiration algorithm using eddy covariance measurements and hydrological modelling in the Rio Grande basin, Hydrol. Sci. J., 58, 1658–1676, doi:10.1080/02626667.2013.837578, http://www.tandfonline.com/doi/abs/10.1080/02626667.2013.837578, 2013.

Sandholt, I., Rasmussen, K., and Andersen, J.: A simple interpretation of the surface temperature/vegetation index space for assessment of surface moisture status, Remote Sens. Environ., 79, 213–224, doi:10.1016/S0034-4257(01)00274-7, 2002.

Santanello, J. a. and Friedl, M. a.: Diurnal Covariation in Soil Heat Flux and Net Radiation, J. Appl. Meteorol., 42, 851–862, doi:10.1175/1520-0450(2003)042<0851:DCISHF>2.0.CO;2, http://journals.ametsoc.org/doi/abs/10.1175/1520-0450(2003)042{\T1\textless}0851:DCISHF{\T1\textgreater}2.0.CO;2, 2003.

Silvestro, F., Gabellani, S., Delogu, F., Rudari, R., and Boni, G.: Exploiting remote sensing land surface temperature in distributed hydrological modelling: The example of the Continuum model, Hydrol. Earth Syst. Sci., 17, 39–62, doi:10.5194/hess-17-39-2013, 2013.

Singh, S. K. and Bárdossy, A.: Calibration of hydrological models on hydrologically unusual events, Adv. Water Resour., 38, 81–91, doi:10.1016/j.advwatres.2011.12.006, http://dx.doi.org/10.1016/j.advwatres.2011.12.006, 2012.

Smith, M. B., Laurine, D. P., Koren, V. I., Reed, S. M., and Zhang, Z.: Hydrologic model calibration in the National Weather Service, Calibration of watershed models, pp. 133–152, 2003.

Spies, R. R., Franz, K. J., Hogue, T. S., and Bowman, A. L.: Distributed hydrologic modeling using satellite-derived potential evapotranspiration, Journal of Hydrometeorology, 16, 129–146, 2015.

Su, Z.: The Surface Energy Balance System (SEBS) for estimation of turbulent heat fluxes, Hydrol. Earth Syst. Sci. Discuss., 6, 85–100, doi:10.5194/hess-6-85-2002, https://hal.archives-ouvertes.fr/hal-00304651/, 2002.

Sun, W., Wang, Y., Cui, X., Yu, J., Zuo, D., and Xu, Z.: Physically-based distributed hydrological model calibration based on a short period of streamflow data: case studies in two Chinese basins, Hydrol. Earth Syst. Sci. Discuss., pp. 1–20, doi:10.5194/hess-2016-192, http://www.hydrol-earth-syst-sci-discuss.net/hess-2016-192/, 2016.

Thom, A. S.: Momentum, mass and heat exchange of vegetation, Q. J. R. Meteorol. Soc., 98, 124–134, doi:10.1002/qj.49709841510, http://dx.doi.org/10.1002/qj.49709841510, 1972.

Tian, Y., Xu, Y.-P., and Zhang, X.-J.: Assessment of climate change impacts on river high flows through comparative use of GR4J, HBV and Xinjiang models, Water resources management, 27, 2871–2888, 2013.

Tramblay, Y., Bouvier, C., Martin, C., Didon-Lescot, J.-F., Todorovik, D., and Domergue, J.-M.: Assessment of initial soil moisture conditions for event-based rainfall–runoff modelling, Journal of Hydrology, 387, 176 – 187, doi:http://dx.doi.org/10.1016/j.jhydrol.2010.04.006, http://www.sciencedirect.com/science/article/pii/S0022169410001873, 2010.

Venegas, P., Grandón, A., Jara, J., and Paredes, J.: Hourly estimation of soil heat flux density at the soil surface with three models and two field methods, Theor. Appl. Climatol., 112, 45–59, doi:10.1007/s00704-012-0705-z, http://link.springer.com/10.1007/s00704-012-0705-z, 2013.

Wan, Z., Zhang, Y., Zhang, Q., and Li, Z.-L.: Quality assessment and validation of the MODIS global land surface temperature, Int. J. Remote Sens., 25, 261–274, doi:10.1080/0143116031000116417, http://dx.doi.org/10.1080/0143116031000116417http://www.tandfonline.com/doi/abs/10.1080/0143116031000116417, 2004.

Wanders, N., Karssenberg, D., de Roo, A., de Jong, S. M., and Bierkens, M. F. P.: The suitability of remotely sensed soil moisture for improving operational flood forecasting, Hydrology and Earth System Sciences, 18, 2343–2357, doi:10.5194/hess-18-2343-2014, http://www.hydrol-earth-syst-sci.net/18/2343/2014/, 2014.

Wang, J. and Bras, R.: Ground heat flux estimated from surface soil temperature, J. Hydrol., 216, 214–226, doi:10.1016/S0022-1694(99)00008-6, http://linkinghub.elsevier.com/retrieve/pii/S0022169499000086, 1999.

Wang, K. and Dickinson, R. E.: A review of global terrestrial evapotranspiration: Observation, modeling, climatology, and climatic variability, Reviews of Geophysics, 50, 2012.

Wang, L., Koike, T., Yang, K., and Yeh, P. J. F.: Assessment of a distributed biosphere hydrological model against streamflow and MODIS land surface temperature in the upper Tone River Basin, J. Hydrol., 377, 21–34, doi:10.1016/j.jhydrol.2009.08.005, 2009.

Wang, L., van Meerveld, H. J., and Seibert, J.: When should stream water be sampled to be most informative for event-based, multi-criteria model calibration?, Hydrol. Res., p. nh2017197, doi:10.2166/nh.2017.197, http://hr.iwaponline.com/content/early/2017/03/13/nh.2017.197.abstracthttp://hr.iwaponline.com/lookup/doi/10.2166/nh.2017.197, 2017.

Xia, D. and Zhang, X.: Construction pattern of distributed real-time flood forecast schemes (In Chinese), J. Hohai Univ. (Natural Sci., 37, 516–522, 2009.

Xu, C.-Y., Gong, L., Jiang, T., Chen, D., and Singh, V.: Analysis of spatial distribution and temporal trend of reference evapotranspiration and pan evaporation in Changjiang (Yangtze River) catchment, Journal of Hydrology, 327, 81–93, 2006.

Yan, H., Wang, S. Q., Billesbach, D., Oechel, W., Zhang, J. H., Meyers, T., Martin, T. A., Matamala, R., Baldocchi, D., and Bohrer, G.: Global estimation of evapotranspiration using a leaf area index-based surface energy and water balance model, Remote Sensing of Environment, 124, 581–595, 2012.

Yao, C., Li, Z.-j., Bao, H.-j., and Yu, Z.-b.: Application of a developed Grid-Xinjiang model to Chinese watersheds for flood forecasting purpose, Journal of Hydrologic Engineering, 14, 923–934, 2009.

Yao, C., Li, Z., Yu, Z., and Zhang, K.: A priori parameter estimates for a distributed, grid-based Xinanjiang model using geographically based information, J. Hydrol., 468–469, 47–62, doi:http://dx.doi.org/10.1016/j.jhydrol.2012.08.025, http://www.sciencedirect.com/science/article/pii/S0022169412007044, 2012.

Yuan, F., Ren, L.-L., Yu, Z.-B., and Xu, J.: Computation of potential evapotranspiration using a two-source method for the Xin'anjiang hydrological model, Journal of Hydrologic Engineering, 13, 305–316, 2008.

Zhang, X. and Lindström, G.: Development of an automatic calibration scheme for the HBV hydrological model, Hydrol. Process., 11, 1671–1682, 1997.

Zhang, X. and Srinivasan, R.: GIS-Based Spatial Precipitation Estimation: A Comparison of Geostatistical Approaches, JAWRA J. Am. Water Resour. Assoc., 45, 894–906, doi:10.1111/j.1752-1688.2009.00335.x, http://doi.wiley.com/10.1111/j.1752-1688.2009.00335.x, 2009.

Zhao, R.-J.: Flood forecasting method for humid regions of China (in Chinese), East China College of Hydraulic Engineering, Nanjing, pp. 19–51, 1977.

Zhao, R.-j.: Hydrological modeling at catchment scale: the Xin'anjiang model and Shanbei model (in Chinese), China Waterpower Press, Beijing, 1 edn., 1984.

Zhao, R. J.: No Title, Xinanjiang Model Appl. China, 135, 1992.

Zhao, R.-J.: Computer models of watershed hydrology, chap. The Xinanjiang model, pp. 215–232, Water Resources Publications, 1995.

Zhou, Y., Zhang, Y., Vaze, J., Lane, P., and Xu, S.: Improving runoff estimates using remote sensing vegetation data for bushfire impacted catchments, Agricultural and Forest Meteorology, 182–183, 332 – 341, doi:http://dx.doi.org/10.1016/j.agrformet.2013.04.018, http://www.sciencedirect.com/science/article/pii/S0168192313000956, 2013.

Figure 1. Flow chart of the XAJ model. The red box denotes the model input consisting of precipitation(P) and pan evaporation (EW); the yellow boxes denote the model simulated fluxes including evapotranspiration (ET) and discharge (TQ); the green box denotes the discharge after routing simulation (usually using the Muskingum method). Symbols outside the boxes are model parameters.
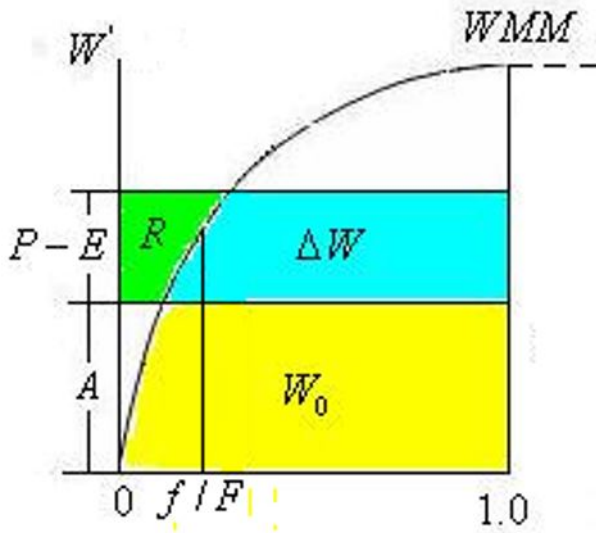
Figure 2. Tension water capacity curve of the XAJ model, which describes the tension water capacity distribution over the catchment. Each point on the curve represents a tension water capacity (Y axis, ranging from 0 to WMM) and the proportion of the area that has a tension water capacity no larger than that value (X axis). The mass balance calculation procedures of the XAJ model are presented: for a given time step when precipitation (P) is larger than evapotranspiration (ET), the difference between P and Evapotranspiration (ET) is partitioned into runoff (R, green shaded area) and soil water (ΔW, blue shaded area) based on the tension water capacity curve and initial soil water (W_0, yellow shaded area)
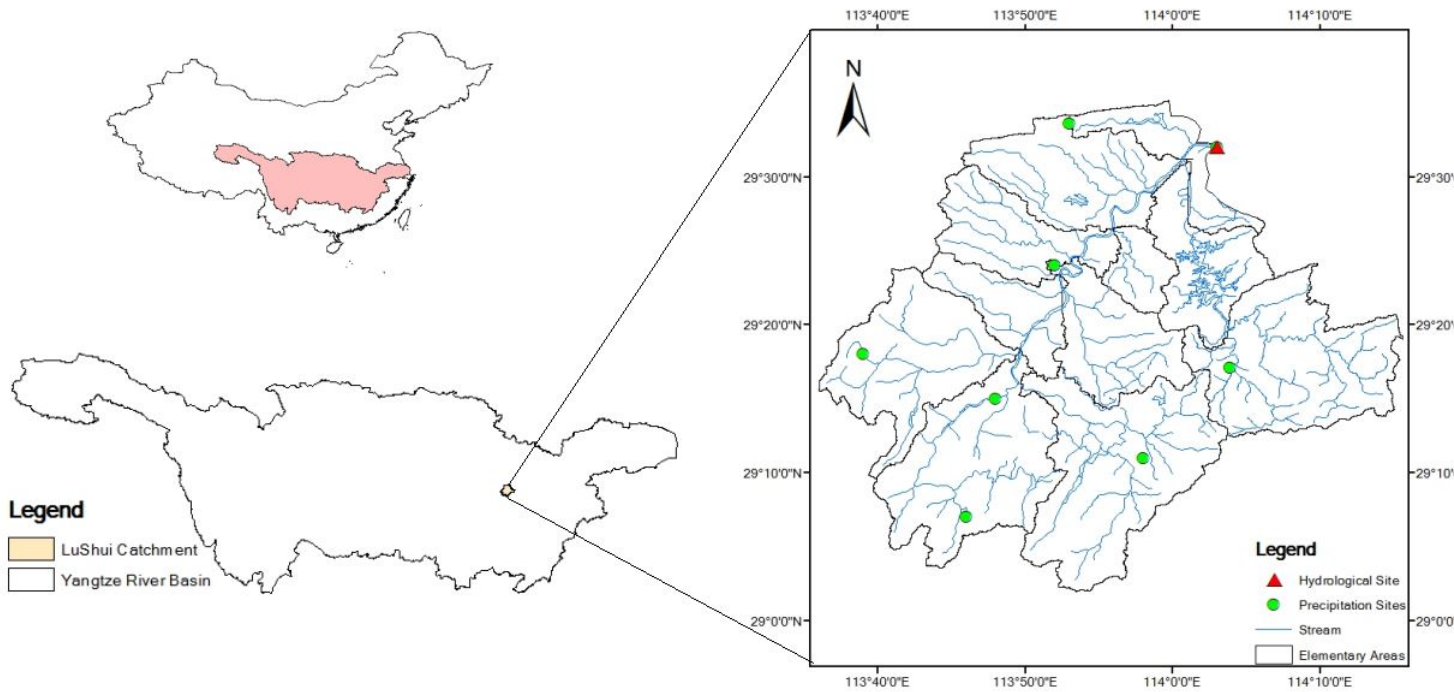
Figure 3. Lushui (LS) catchment. The red triangle is the ChongYang hydrological site that observes precipitation, pan evaporation and runoff; the green dots are precipitation sites set up to measure precipitation only; the blue line is the LS stream. The elementary areas are also shown, which are the computation unit of the XAJ models (see Section 2.1 for details).
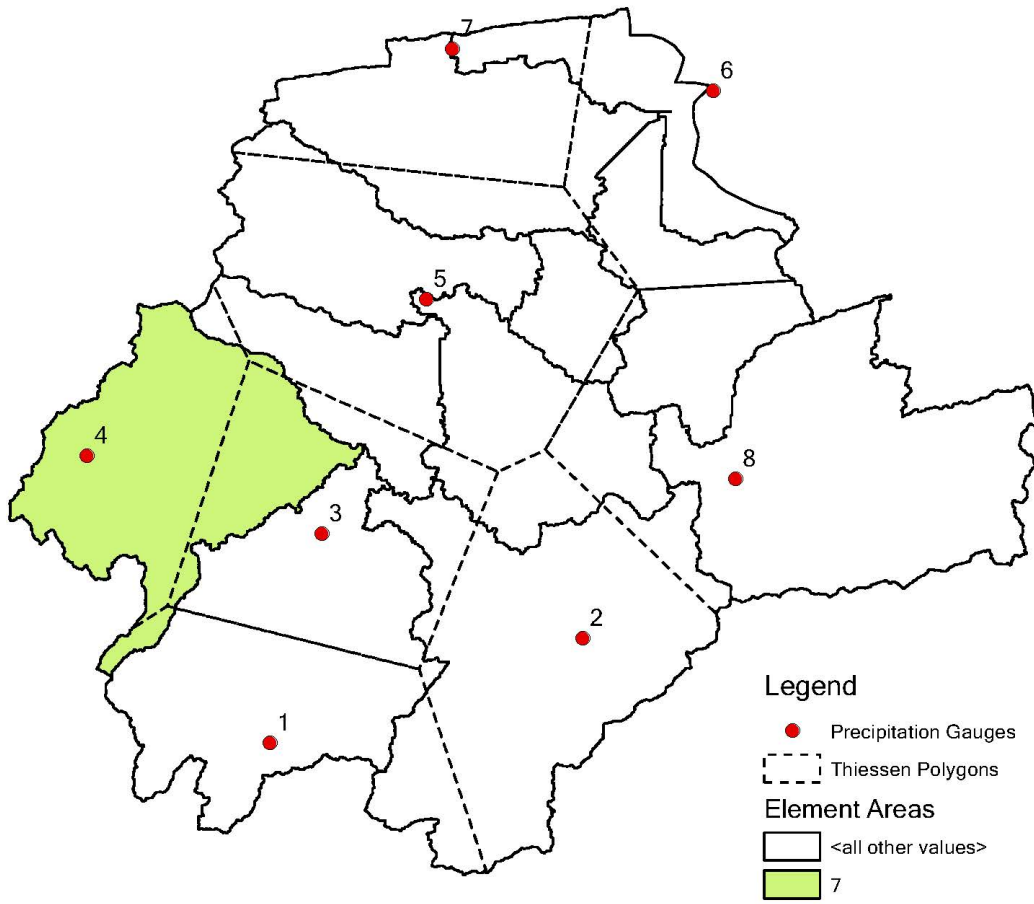
Figure 4. Sketch plot of precipitation calculation based on element areas and Thiessen polygons.
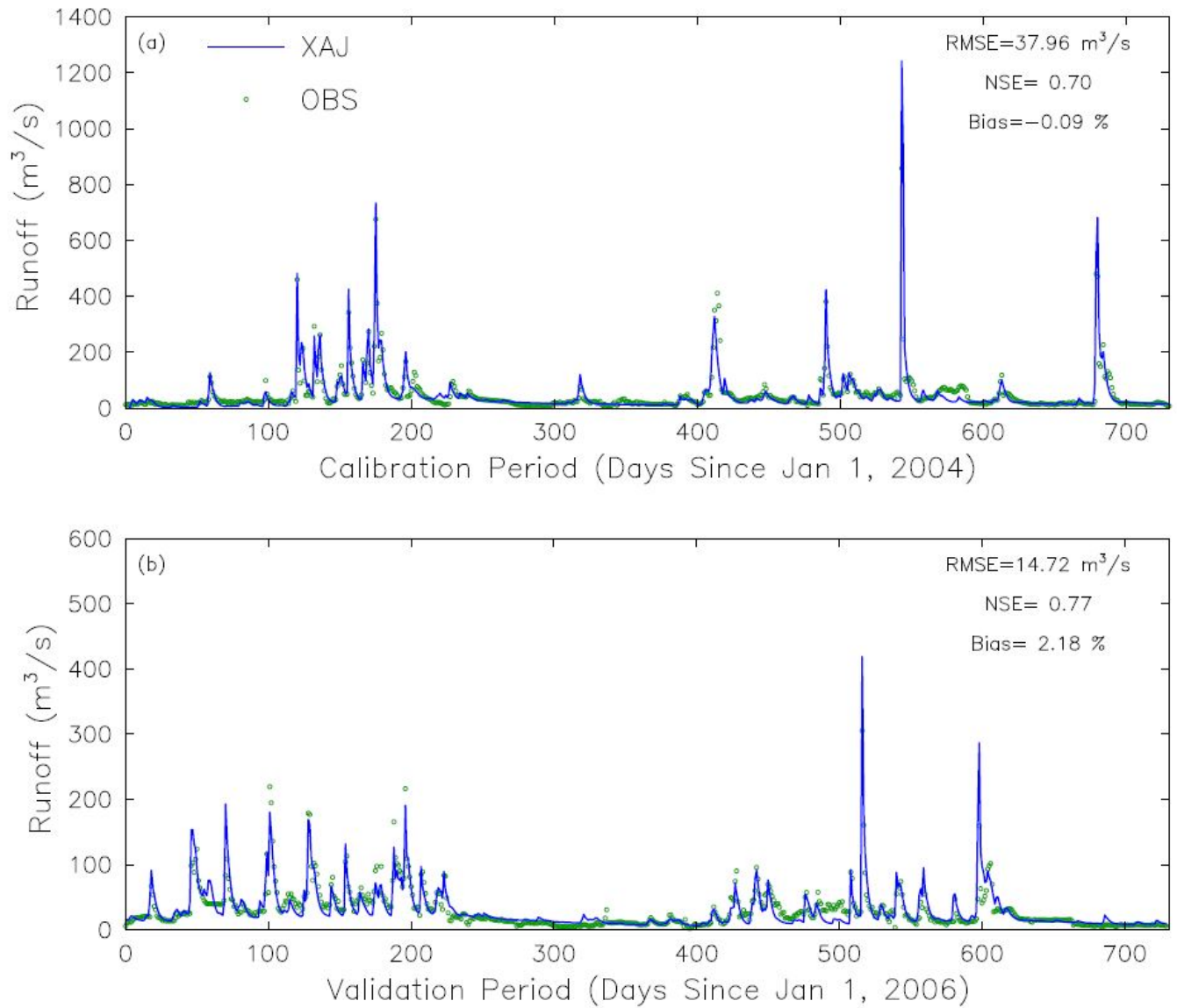
Figure 5. Comparison between observed and XAJ-modeled daily runoff for the ChongYang hydrological site for the calibration (a; Jan 1, 2004–Dec 31, 2005) and validation (b; Jan 1, 2006–Dec 31, 2007) period. Also shown the evaluation metrics including: RMSE, NSE, and bias.
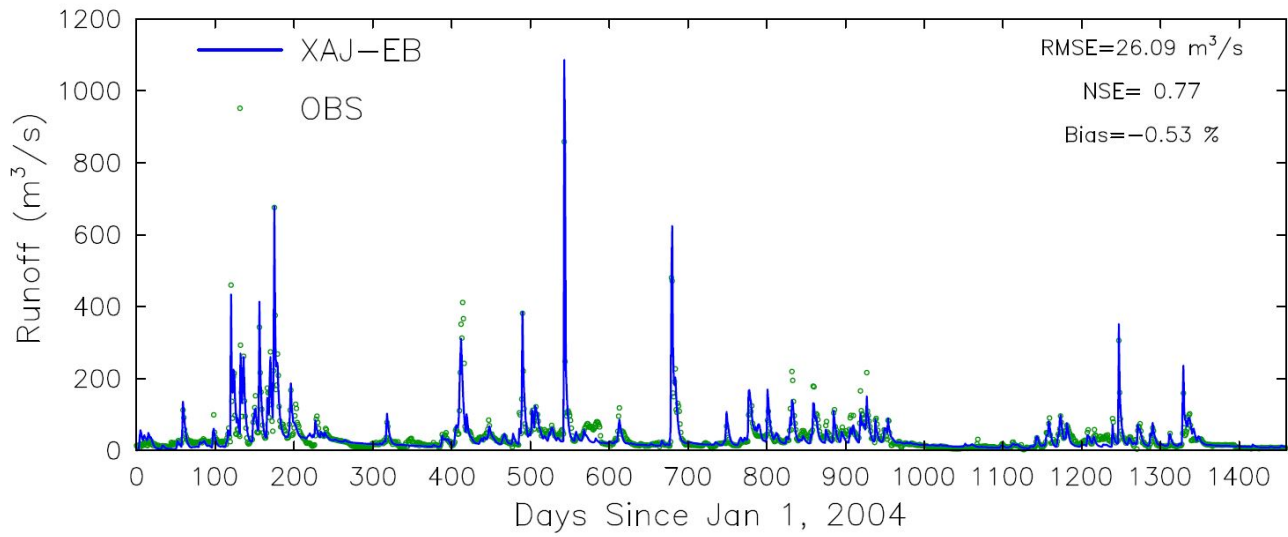
Figure 6. Comparison between observed and XAJ-EB modeled daily runoff for tue ChongYang hydrological site for period between Jan 1, 2004–Dec 31, 2007. Also shown the evaluation metrics including: RMSE, NSE, and bias.
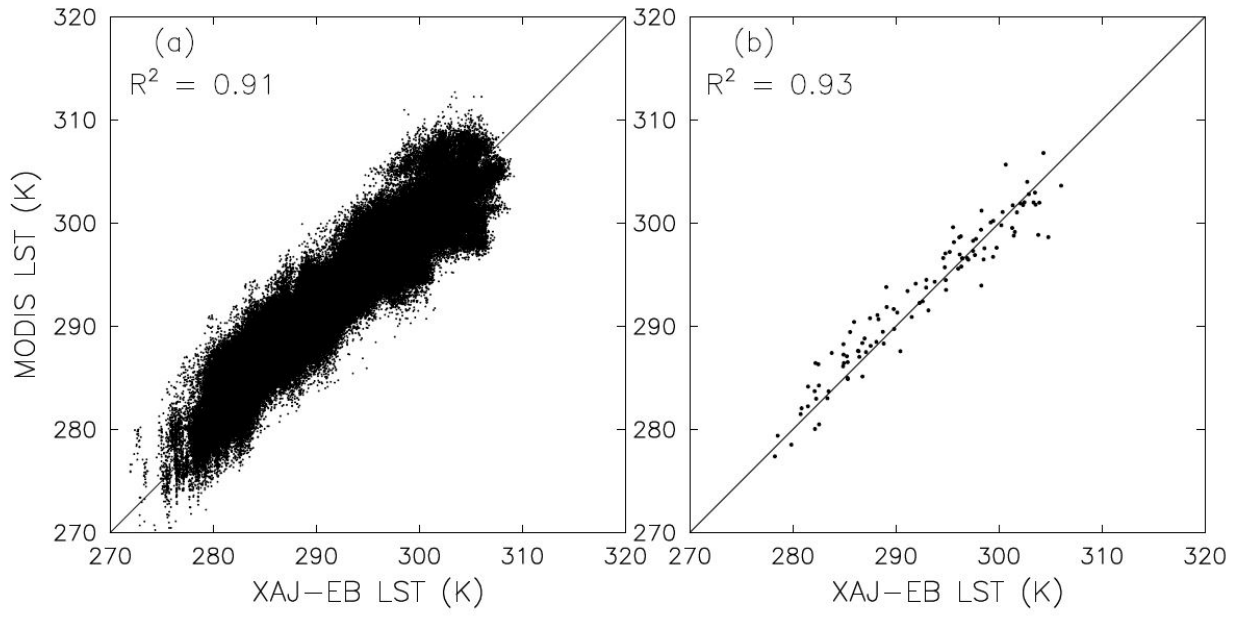
Figure 7. Scatter plot of MODIS retrieved and XAJ-EB modeled land surface temperature (LST), (a): catchment average LST and (b): grid LST.
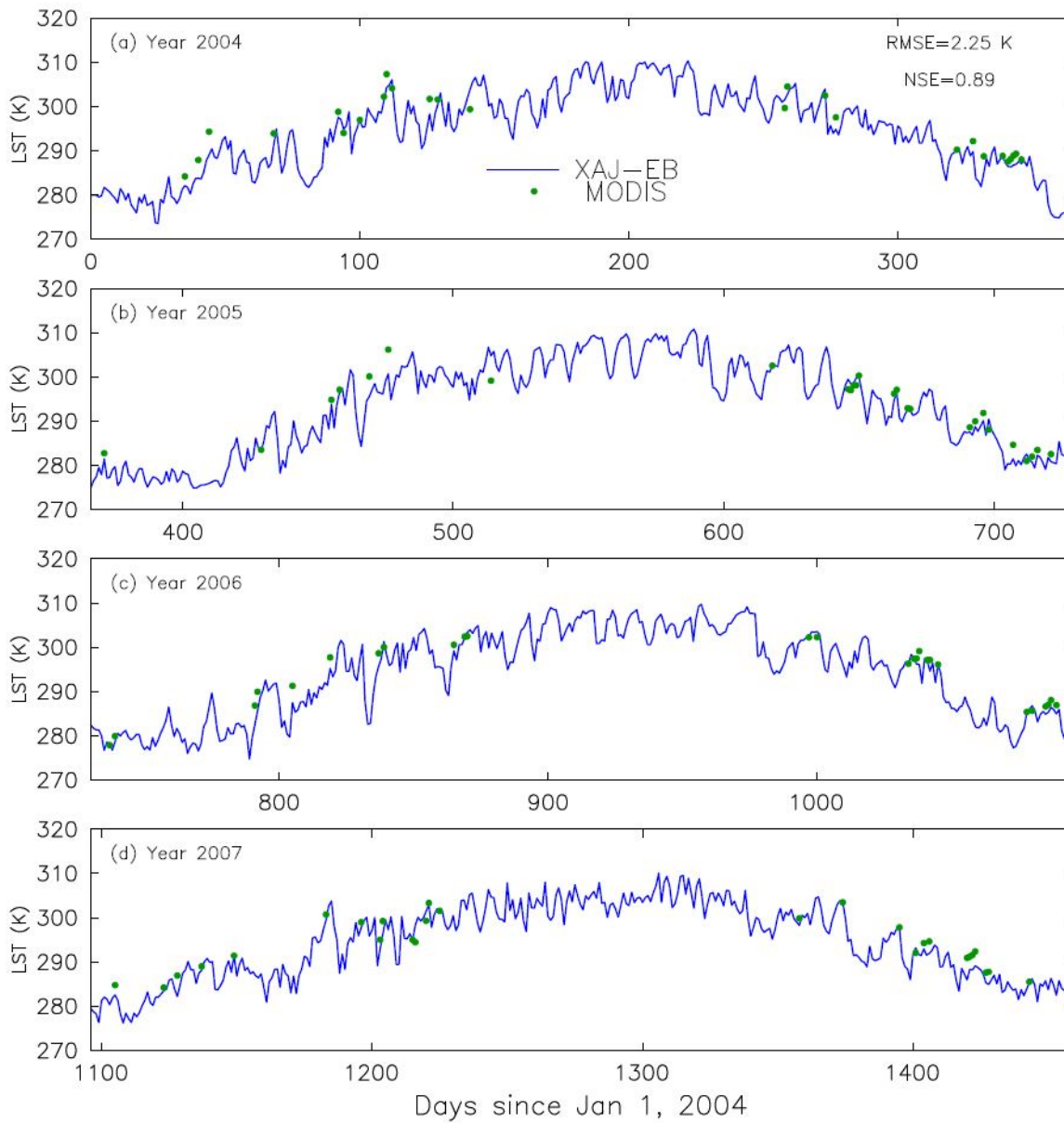
Figure 8. Time series of modeled catchment average land surface temperature for the period between Jan 1, 2004–Dec 31, 2007. The MODIS-retrieved catchment-average land surface temperature (LST) is also shown when the data availability exceeded the threshold(see Section 3 for details).
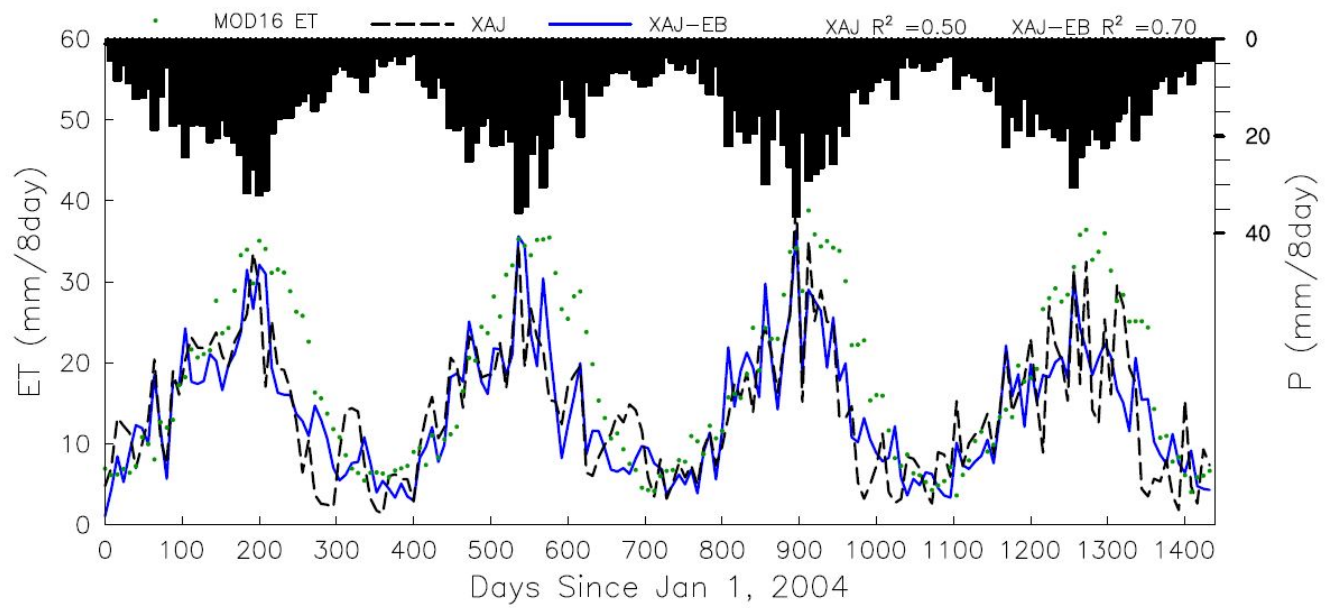
Figure 9. Comparison among MODIS-retrieved, XAJ and XAJ-EB-modeled 8-day catchment-average evapotranspiration (ET) for period between Jan 1, 2004–Dec 31, 2007. The 8-day gauge-measured catchment-average precipitation is also shown for the same period.
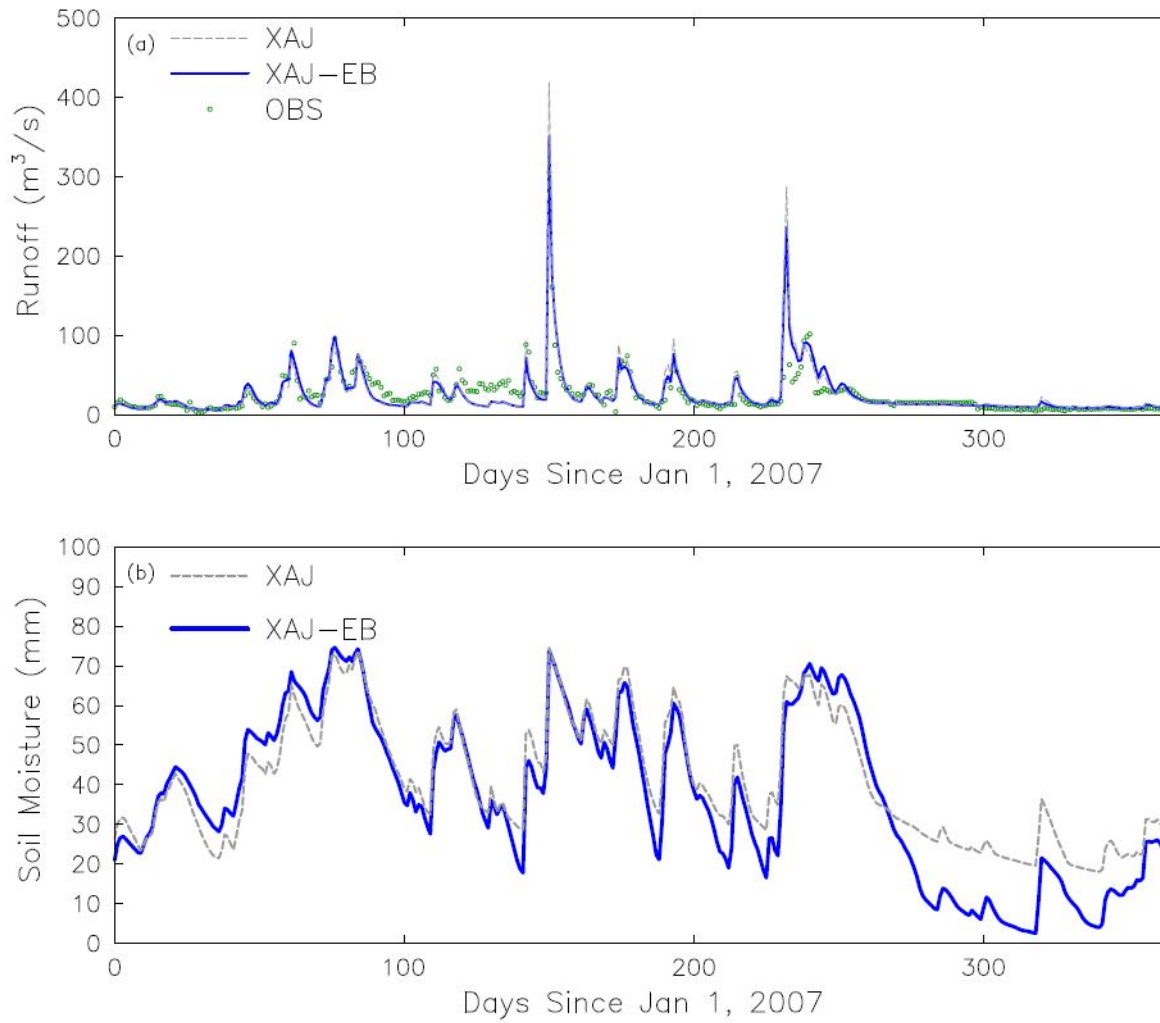
Figure 10. Comparison between XAJ and XAJ-EB modeled daily runoff (a) and soil moisture (b) for the yea 2007, soil moisture is expressed as equivalent water depth (soil depth * volumetric soil moisture) as defined by the XAJ model.
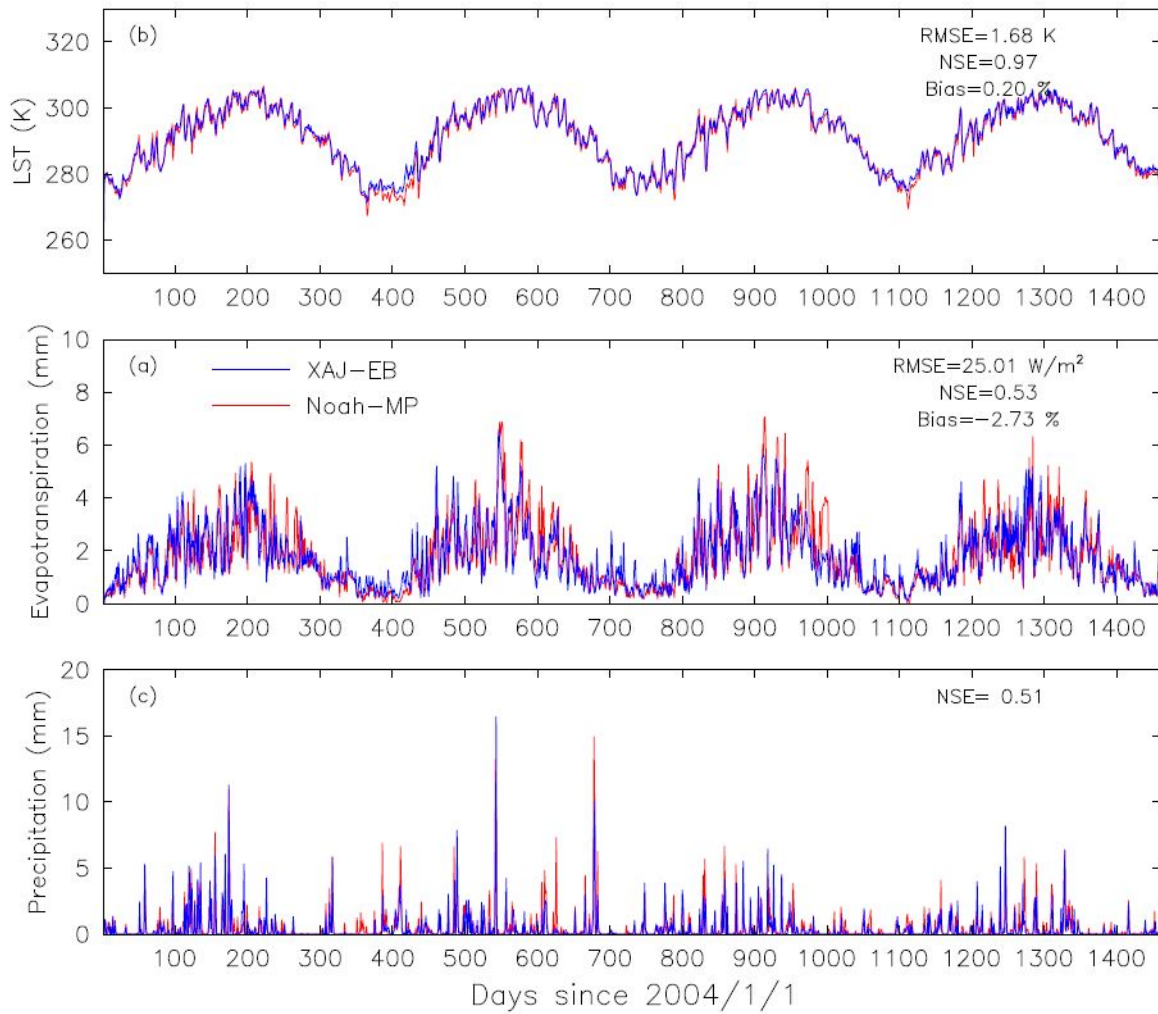
Figure 11. Comparison between XAJ-EB and Noah-MP modeled catchment average latent heat flux (a) and land surface temperature(b). (c) illustrates the comparison between catchment average precipitation used by XAJ-EB and Noah-MP.

Table 1. Parameter symbols and corresponding definitions in the XAJ model, Also shown the parameters calibrated for Lushui(LS) catchment during year 2004 and 2005.

Parameter	Definition	Calibrated Value for the LS Catchment
IMP	Ratio of impermeable area to the total area in the catchment	0.01
KC	Ratio of potential evapotranspiration to pan evaporation	0.95
B	Exponential of the distribution of tension water capacity	0.50
WM	Elementary area mean tension water capacity	Vary
WUM	Tension water capacity of upper layer	Vary
WLM	Tension water capacity of lower layer	Vary
C	Deeper evapotranspiration coefficient	0.10
SM	Elementary area mean free water capacity	45.00
EX	Exponential of the distribution of free water capacity	1.50
KG	Outflow coefficient of free water storage to the ground flow	0.40
KI	Outflow coefficient of free water storage to the sub-flow	0.40
CI	Recession constant of sub-flow storage	0.63
CG	Recession constant of groundwater storage	0.99
CS	Recession constant during stream routing in the elementary area	0.55
LAG	Lag time step during stream routing in the elementary area	0

Table 2. Variable, MODIS product name and spatial and temporal resolution of the remote sensing data used in this paper

Remote Sensing Variable	MODIS Product Name	Spatial Resolution	Temporal Resolution
LAI	MCD15A3	1 km	4-day
Albedo	MCD43A1	500 m	16-day
LST	MOD11A1	1 km	Daily
ET	MOD16A2	1 km	8-day